STRUCTURAL DYNAMIC AND INHERENT DAMPING CHARACTERIZATION OF ADDITIVELY MANUFACTURED AIRFOIL COMPONENTS

THESIS

Andrew W. Goldin, 1st Lt, USAF

AFIT-ENY-MS-20-M-263

DEPARTMENT OF THE AIR FORCE
AIR UNIVERSITY

AIR FORCE INSTITUTE OF TECHNOLOGY

Wright-Patterson Air Force Base, Ohio

DISTRIBUTION STATEMENT A
PUBLIC RELEASE; DISTRIBUTION UNLIMITED.

AFIT-ENY-MS-20-M-263

STRUCTURAL DYNAMIC AND INHERENT DAMPING CHARACTERIZATION OF ADDITIVELY MANUFACTURED AIRFOIL COMPONENTS

THESIS

Presented to the Faculty

Department of Aeronautics and Astronautics

Graduate School of Engineering and Management

Air Force Institute of Technology

Air University

Air Education and Training Command

In Partial Fulfillment of the Requirements for the

Degree of Master of Science in Aeronautical Engineering

Andrew W. Goldin, BS

1st Lt, USAF

March 2020

AFIT-ENY-MS-20-M-263

STRUCTURAL DYNAMIC AND INHERENT DAMPING CHARACTERIZATION OF ADDITIVELY MANUFACTURED AIRFOIL COMPONENTS

Andrew W. Goldin, BS

1st Lt, USAF

Committee Membership:

Dr. R. G. Cobb
Chair

Maj R. A. Kemnitz, PhD
Member

Dr. O. E. Scott-Emuakpor
Member

Dr. T. J. George
Member

Abstract

The push for low cost and higher performance/efficient turbine engines have introduced a new demand for novel technologies to improve robustness to vibrations which often result in High Cycle Fatigue (HCF). There have been many proposed solutions to this, some passive and some active. With the advent of Additive Manufacturing (AM), new damping techniques can now be incorporated directly into the design and manufacture process to suppress the vibrations that create HCF. Recent work performed by Scott-Emuakpor et al. used powdered filled pockets within a beam structure to act as a damping mechanism to increase the structural damping. This method has shown success, with up to 95% forced response reduction when using 1-3% unfused powder within the pocket volume. The corresponding strain limit due to the increased damping was found to be between 300 and 700με. Also noted was that the damping effectiveness does not return after the strain is reduced, but was observed to be relatively steady in the measured damping quality factor after the initial loss. The next step in this investigation is to apply the technology to blade structures. In this study, this novel unfused pocket damping technology is applied to a blade structure and the resulting damping effectiveness is quantified. The application of this technology to complex geometries will provide insight into both the underlying damping mechanism and its overall effectiveness. The blades are manufactured using a laser powder bed fusion process with Inconel 718. An intentional void is left in each blade to serve as the internal pocket which remains filled with unfused powder as part of the regular AM building

process. The finished blades are then computed tomography (CT) scanned to determine the as manufactured fill volume and to verify initial powder locations. In this research, first the damping quality is investigated when this technology is applied to a fan-like blade. Second, the strain limitations are investigated to determine if they are similar to that previously observed by Scott-Emuakpor et al. and if they are affected when the blades are tested in representative operating temperatures for both sub-sonic and supersonic post inlet conditions. To accomplish the tests, both solid and pocketed blades at room temperature are tested followed by testing at elevated temperatures. All damping tests were conducted using an electrodynamic shaker and a convection furnace for the elevated temperatures. Post-test, the blades were CT scanned again and compared to the pre-test scans, to ascertain the state of both the powder and the blades as a whole. This research allowed an initial evaluation of the effectiveness of this technology to turbine engine fans as well as highlighting the overall effectiveness of this type of passive damping. The research herein expands the potential of this technology and takes the first steps to towards applications in rapid manufacturing of components with a highly effective inherent passive damping capability.

Acknowledgments

I would like to express my sincere appreciation to my faculty advisor, Dr. Richard Cobb, for his guidance and support throughout the course of this thesis effort. The insight and experience was certainly appreciated. I would like to thank the AniMal Lab for manufacturing the blades, and CT scanning. Also the AFIT machine shop for final machining. I would, also, like to thank my sponsor and committee members at the Turbine Engine Fatigue Facility, Dr. Tommy George & Dr. Onome Scott-Emuakpor, for both the support and assistance provided to me in this endeavor. Not to mention the members of the TEFF government and contractors who helped me considerable in this work effort. Most importantly I could not have done this without the support of my wife Meagan who endured my weird hours, tired/frustrate state, and helped me supported me in uncountable ways.

Andrew W. Goldin

Table of Contents

Page

List of Figures

Page

List of Tables

Page

STRUCTURAL DYNAMIC AND INHERENT DAMPING CHARACTERIZATION OF ADDITIVELY MANUFACTURED AIRFOIL COMPONENTS

I. Introduction

General Introduction

In the 1980's and 90's the U.S. Air Force had a number of class A engine failures due to High Cycle Fatigue (HCF). These engines had inserted blades, and at this time the Air Force was moving to use Integrally Bladed Disks (IBD, IBR, Blisks). The loss of the blade to disk interaction which created damping through friction is now the main cause of these issues (Bartsch T. M., 2002). This cased alarm as the engine that had failed due to HCF were inserted disk and it was becoming know that the problem would be much worse in IBD's. Many different methods have been used to attempt to limit HCF failures. All methods have pros and cons with respect to both cost and performance. With the onset of additive manufacturing (AM) new concepts have started to arise for solving the HCF issue. The AM inherent damping method developed by (Scott-Emuakpor, George, & Runyon, 2018 Pending) which incorporates powder filled pockets is the first low cost, low interaction method. In (Scott-Emuakpor O. , et al., 2019) it is shown that with only 1% of volume used for the pockets you can achieve 95% forced response reduction in beams. However there has been an observed loss of damping quality during and after high strain cycles. This has been investigated in (Scott-Emuakpor O. , et al., 2019) which showed that after 700 με the loss of damping quality is repeatable. The cause of this loss of damping is under investigation and is currently thought to be based on the significant friction in the powder causing the powder to create

heat and fuse. This fusing increases at high strain causing clumps of powder to be created and thus loss of damping quality.

The aerospace industry has long sought weight reduction, which would allow improvement in system performance while maintaining structural integrity. In the case of turbine engines, this conflict of tradespace between weight reduction and structural integrity is complicated by rotating componentry. Specifically, the inserted airfoil and disk combinations seen in most of the legacy fleet are seldom preferred to integrally bladed disks (IBDs) in modern engine design due to significant weight benefits. Yet, despite the performance benefits provided by IBDs, a notable detriment is the loss of damping from the airfoil-to-disk energy dissipation via friction. The lack of this interaction increases the susceptibility of IBDs to high amplitude vibration, increasing the risk of High Cycle Fatigue (HCF) that can lead to engine failure. The possibility of such an event is why HCF is addressed from the beginning of conceptual design throughout the lifecycle of critical parts like IBDs (U.S. Air Force, 2002; Nicholas, 2006; Danforth, 1975). The intent during design is to manufacture IBDs that keep HCF-inducing frequencies outside of engine operational speeds. This is a non-trivial task; therefore, HCF mitigating efforts such as increased manufacturing scrutiny and vibration suppression are considered to sustain the durability of IBDs during operation, as well as significate engine instrumentation for testing and validation of design. The latter, vibration suppression, has been investigated for a number of years and yielded innovative approaches such as viscoelastic treatments, damping coatings (ceramic and metallic based), as well as impact and friction dampers (Nashif, Jones, & Henderson, 1985; Torvik, Patsias, & Tomlinson, 2002; Lopez, Busturia, & Nijmeijer, 2004; Olson, 2003;

Jones & Parin, 1972; Torvik P. J., 2010; Panossian, 1991) (Torvik P. J., 2011; Reed, 2007; Scott-Emuakpor, et al., 2016; Torvik & Langley, 2015; Torvik, Wilson, & and Hansel, 2007,; Els, 2011; Sinha & Griffin, 1983) (Nashif, Torvik, Desai, Hansel, & Henderson, 2008). Although each method has been proven effective, all have shortcomings that make them problematic for turbine engine applications. Phenomena such as stress concentrations can create structural integrity challenges that encroach on the tradespace associated with weight reduction.

Problem Statement

The Air Force has pushed for rapid prototyping and manufacturing to reduce cost and improve readiness. When AM techniques are applied to gas turbine engines, many issues present themselves. Chief among them is safety of flight issues such as HCF and thus the Air Force needs a new and novel damping method or technology to allow for rapid manufacturing and prototyping of turbine engines.

Research Hypotheses

The technology introduced above of adding inherent damping to additive manufacturing using powdered pockets can be applied to this problem. To support this hypothesis, first this technology must be applied to the complex structure of a turbine engine blade. Secondly the damping performance must be evaluated and compared to a structure manufactured without this technology. This evaluation must be done both at room temperature, for technical understanding and comparison to other studies, and at relevant supersonic fan temperatures for the eventual applications. This research will lay

the framework for this novel invention to be applied to many different complex structures.

Investigative Questions

The research questions to be answer are threefold. First, can inherent damping of additive manufacturing be applied to the complex structure of a turbine engine blade? Second, are there strain limitations of this technology? Third, does temperature affect either of the first two questions? The strain limitations will be defined as the strain at which the quality factor (Q)[1] increases significantly from the initial damping state which is a decrease in damping.

Research Tasks

The research necessary to support the hypothesis will be performed in the following six research tasks. The first task is to design a blade that is generic but also relevant in complexity to real application. Second, investigate the physical structure. Third, investigate the damping capability. Fourth, understand the dynamic behavior as it changes through strain amplitude testing. Fifth, investigate elevated temperature effects on endurance and damping. Lastly, investigate if the physical structure or the dynamic behavior changed.

Methodology

In order to accomplish the research tasks, multiple types of tests will have to be performed. The parts will be physically investigated through structured light scanning, to

[1] Damping is commonly measured using the 'Q' factor where low Q indicates high level of damping.

obtain external geometry, and Computer Tomography (CT) scans to understand internal structure. The dynamic behavior will be studied using modal analysis and by studying the damping performance. A sinusoidal dwell test will be used to strain the part to allow an understanding of its strain limitations. Next, the aforementioned tests will be repeated to see if results are repeatable and consistent.

Assumptions/Limitations

There are both time and financial limitations. Ideally a large number of blades both pocketed and solid could be manufactured and tested, but this would incur large costs and take substantial amount time. For this initial study, 6 pocketed blades and 3 solid blades will be used to demonstrate this method.

Due to this limited number of parts, only one elevated temperature will be investigated, 400°F, and will be used to understand if there is any change in strain amplitude. The aforementioned temperature is relevant to the supersonic cruise missile size class engine.

This technology takes advantage of a ‘drawback’ of Laser Powered Bed Fusion (LPBF) that is that internal volumes will have powder deposited in them during the build. For this study these parts will not undergo standard post processing for LPBF, to include heat treatment. This is because the heat treatment would sinter the powder which would reduce its freedom of motion therefore reducing if not negating the damping affects sought after in this study. The primary downside of not undergoing heat treatment is a decrease in potential strength which has Low Cycle Fatigue (LCF) implications. This

limitation is lessened when the ideal application is in expendable gas turbine engines as the typical LCF cycles is very low due to the short operational timeframes.

Implications

If successful this study will lay the groundwork for incorporating damping into the rapid manufacture and prototyping of turbine engine components and has potential for even an entire turbine engine. This study will also show the general utility of this technology which could lead to its application in a wide variety of structures from automotive to space.

Preview

The study herein attempts to show the viability of applying the AM powder pocket technology to complex structures and lays the framework for its application to other complex structures for vibratory response reduction. Having defined the problem above, Chapter 2 provides an overview of the problem space and potential solutions. Chapter 3 develops the means and methods used to experiment and investigate the technology. Chapter 4 provides analysis and results of the tests performed and Chapter 5 lays out the conclusions and recommendations of the research.

II. Background

Chapter Overview

This chapter outlines both the problems and possible solutions the Air Force has had with High Cycle Fatigue (HCF). The potential solutions that have previously been investigated will be outlined briefly and presented with their benefits and drawbacks.

Problem Background

The Air Force HCF failure issues were notable during the 80's and 90's after the initial introduction of IBRs into regular use in gas turbine engines. These issues presented themselves and the Air Force's response was the creation of the HCF initiative. This initiative was a joint venture with both DOD and non-DOD government, industry and international partners through the Joint Strike Fighter (JSF) program. "Between 1982 and 1996, high cycle fatigue accounted for 56% of Class A engine-related failures. HCF is a major factor negatively impacting safety, operability, and readiness, while at the same time increasing maintenance costs. In fiscal year 1994, HCF required an expenditure of 850,000 maintenance man-hours for risk management inspections. Estimates put the cost of high cycle fatigue at over $400 million per year." (Bartsch T. M., 2001) The HCF action teams looked into a multitude of different solutions to these problems. Their best practice document focuses mainly on the processes to follow in testing and development of a gas turbine engine (Fecke, et al., 2005) which comes down to relying on the deterministic parameters like 60% Goodman[2] for engine safety.

[2] 60% Goodman (or Haigh) diagram refers to a plot of vibratory vs steady stress where data is plotted for a constant number of fatigue cycles which for Goodman Diagrams is all 10^7 cycles (U.S. Air Force, 2002; Nicholas, 2006)

Currently, the Department of Defense (DoD) and industry are reaching for improved performance and reducing costs and are investigating ways of doing this. Specifically for expendable engines the DOD is looking at 'targeted life' engines or short life engines. This concept is based on the premise that we don't want to pay for any extra life than is needed. For instance if a cruise missile engine's mission is nominally one hour and design life of that engine should be 10 or 20 hours. If the community can do this we can make the production of this engine less expensive since the extended life and deterministic practices typically require the engine to need more material which creates weight and cost increases. This design concept is called 'targeted life' and is significantly harder than it may appear. Since the engineering ability to make such hardware is so complex, to have something break right at 20 hours and not have extra life is very challenging. In this solution the overall bulk of the engine is decrease which increase the induced vibration related stress. There is where the damping technology is most needed and can be applied to a cheaply produced engine. This damping technology would need to be unobtrusive so it does not add much weight, if at all, and does not affect performance. To fully explore potential solutions, the following sections will overview a number of technologies aimed at solving the HCF issue.

Coatings

During the HCF program, coatings were looked into as a possible damping mechanism for turbine engines. The technology of coatings is still undergoing efforts and due to the large number of material possibilities has a vast set of tests to fully understand. The Turbine Engine Fatigue facility (TEFF) did a study of a few coatings

documented in the 2001 HCF annual report and found that relationships of Q to strain: "A system Q = 900 at 10 micro-strain units, Q = 200 at 100 units, and Q = 120 at 400 units are typical of results obtained." (Bartsch T. M., 2002, p. 135)

Bartsch showed that coatings can work well as a damper in turbine engines and even the potential added benefit for the hot section of providing a thermal barrier. However, the added mass, surface finish and the geometric change to the part can greatly affect aerodynamic performance and total weight. This has led to only limited use in modern turbine engines.

Particle Dampers

Particle dampers use the interactions through impact or friction of the particles within a confined space to extract energy from the vibratory mode. Studies done during the HCF program on particle damping found that Q's of 122 to 73.5 during the test period data seen in Figure 1. These particle dampers used 80 internal particles and were tested at multiple amplitudes. (Bartsch T. M., 2001)

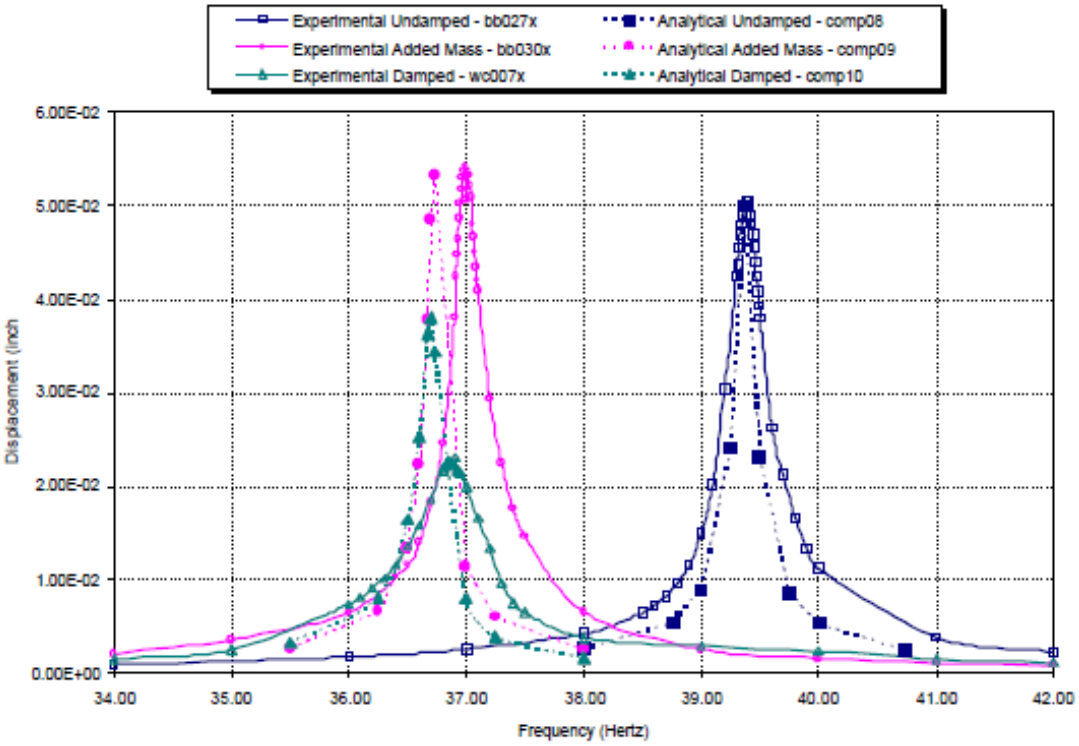

Figure 1: Comparison of Experimental and Analytical Results. **(Bartsch T. M., 2001)**

A similar damping method was done by NASA using a self-tuning impact damper seen in Figure 2. NASA demonstrated results with as much as 50% resonate peak reduction. These tests were done at the Dynamic Spin Rig Facility at NASA Glenn Research Center. (Bartsch T. M., 2003)

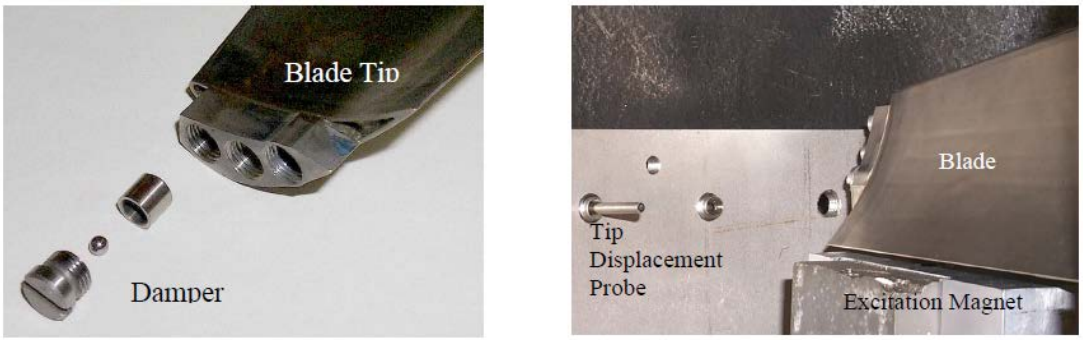

Figure 2: (a) Self-Tuning Impact Dampers and (b) Dynamic Spin Rig Facility, NASA Glenn Research Center **(Bartsch T. M., 2003)**

Altogether, particle and impact dampers were tested both at bench level as well as under centrifugal loads. These tests found significant damping and, as shown by NASA, are self-tuning and passive. The problem with implementing this technology lies in incorporating it into the blade architecture as well as the added mass. The life, and life impacts, of this style of damper also has not been well studied nor fully understood for turbine engine applications.

Air Film & Foil Dampers

Air film and foil damping systems were also studied during the HCF program. Specifically the Air Film Damping System (AFDS) was installed on fan blades and tested. The AFDS works by having an air pocket with an outgas hole where the air is pumped in and out by the vibratory motion. A similar concept using just a foil attached to the blade with adhesive also works but is much less effective, Figure 3 shows one such test in both vacuum and ambient air pressure. In ambient pressure a Q of 20 was found and in vacuum a Q of 212.7 was found for the targeted two stripe mode (2-S). The

report states that the comparison between these two tests show evidence that the AFDS was effective. Figure 4 shows this same technology compared to a baseline blade. The manufacturing process is described thusly:

“In essence, a pocket is milled in the fan blade. A separate cover platelet is attached via structural adhesive or metallic bond. A specific air film gap is maintained between the AFDS platelet and the fan blade.” (Bartsch T. M., 2002, pp. 141-150)

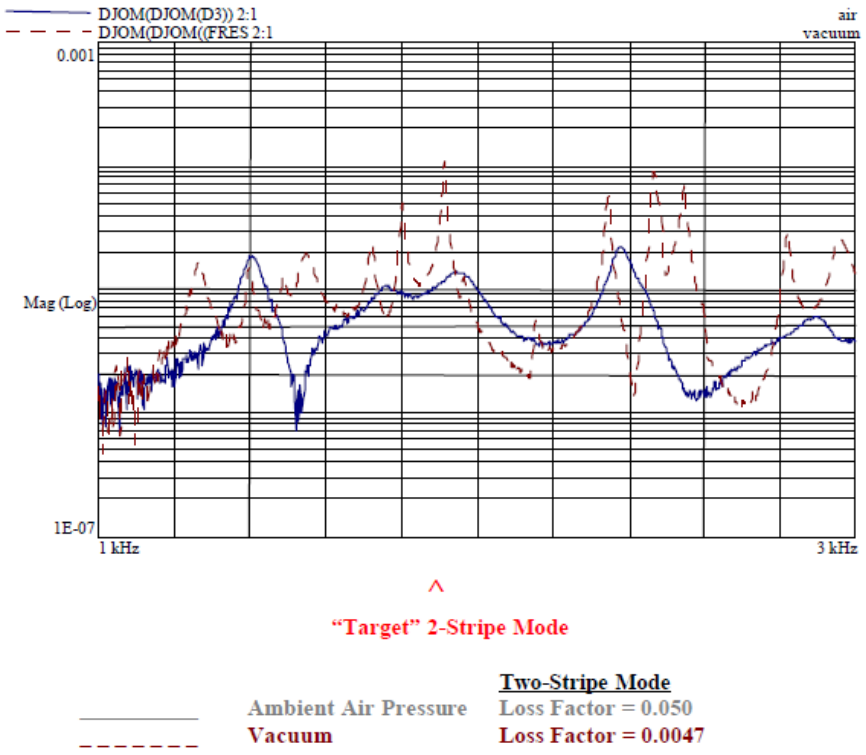

Figure 3: External Titanium Air Film Damping Systems Applied to the GMA3007 Type III Fan Blade (Experimental results) (Note: Y-axis Uncalibrated) **(Bartsch T. M., 2001)**

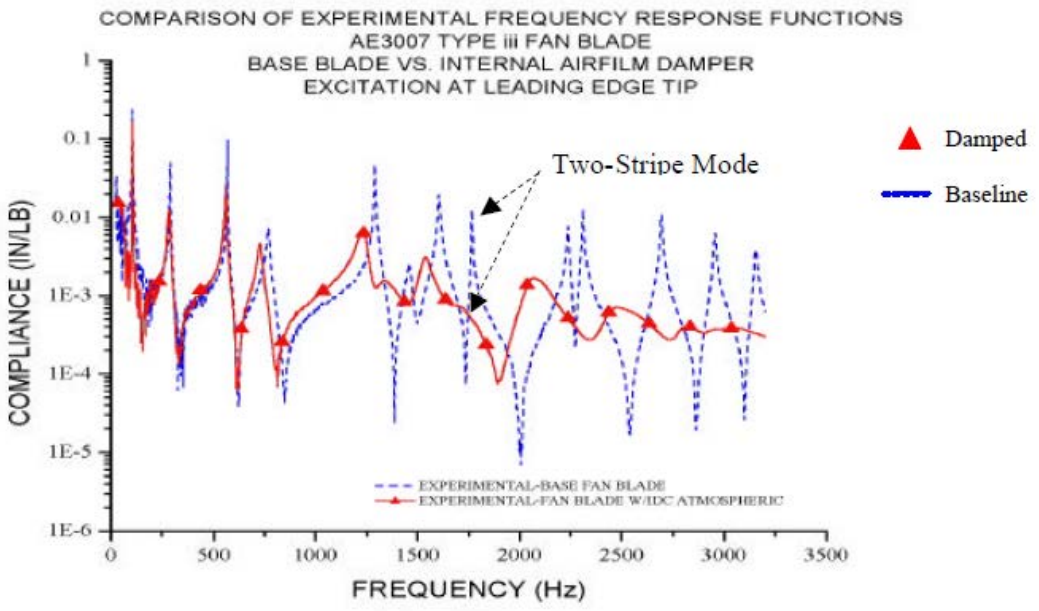

Figure 4: Measured AFDS Performance **(Bartsch T. M., 2002)**

A similar technology called constructive layer damping system which involves a film with adhesive attach to the bade showed similar effectiveness. However, there have been multiple accidents in which the film has detached due to inadequate bonding and created a domestic object damage (DOD) incident in the engine sometimes resulting in engine damage and increased maintenance activity, the exact problem they were attempting to sole.

Viscoelastic Dampers

A viscoelastic material study was done on the AE3007 fan blades and reported on in the 2001 HCF program report. This study tested viscoelastic material that was inserted in a similar manner to that of the airfoil above, and studied Q change over a temperature range. The damping data is shown in Figure 5 and Figure 6 (Bartsch T. M., 2002, pp.

124-126). This data shows that the viscoelastic material had significant damping and the temperature effect on that damping. Because viscoelastic materials are temperature dependent they are often used in layers so that their damping capability can be optimized for multiple temperatures. The main drawback of viscoelastic material is in how it is applied, many attempts at internally filled or partially filled blades result in blow out (when centrifugally loaded) or bond failure of the adhesive material. The internal filling is also a difficult manufacturing process and is normally very time consuming.

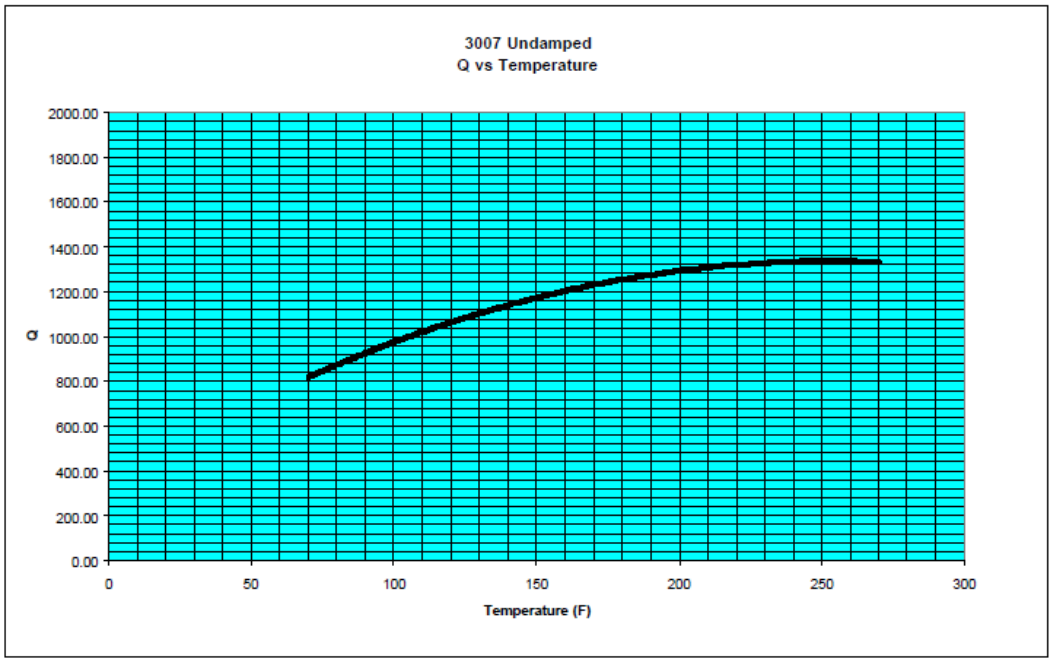

Figure 5: Undamped AE3007 Blade Bench Test **(Bartsch T. M., 2002)**

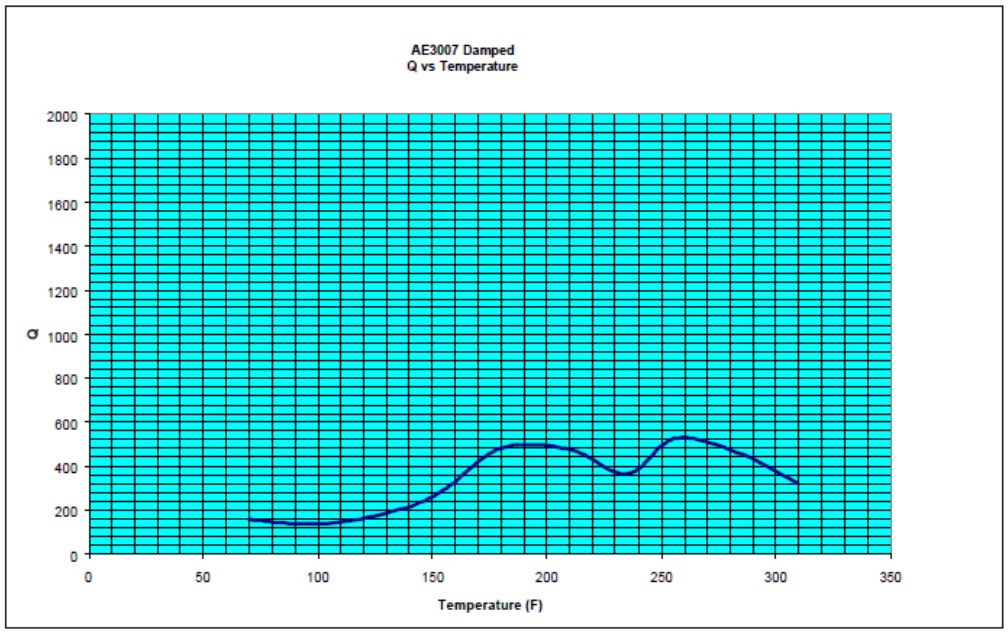

Figure 6: AE3007 Damped Blade #807 Bench Test Results **(Bartsch T. M., 2002)**

Additive Manufacturing Damping Synopsis

The lack of a viable application to reduce IBD weight while suppressing HCF vibration has led to the exploration of the capabilities provided by additive manufacturing (AM). Using the Laser Powder Bed Fusion (LPBF) AM process, components with unique internal geometries can be manufactured, and the densely packed powder trapped within these internal geometries can provide inherent damping of the part. This concept has been validated in three separate studies with Inconel (IN) 718 beams. In the first study, the unfused pockets in beams demonstrated an amplitude suppression of 90% while only altering the fused volume of the part (unfused pocket) by 1–4% (Scott-Emuakpor O. , et al., 2018). The second study demonstrated a similar damping capability: 90% amplitude reduction using only 1% unfused pocket volume (Scott-Emuakpor O. , et al., 2018; Scott-

Emuakpor O. , George, Runyon, & O'Hara, 2018) Although the initial (before endurance or high strain testing) damping capabilities demonstrated by each study are encouraging, there appears to be a degradation of the damping capability at either higher strain amplitudes and/or longer sweep durations. The third study focused on endurance and found loss of damping quality between 300 με and 700 με, in addition, damping quality did not return after low strain sweeps or other methods attempted at releasing the powder (Scott-Emuakpor O. , et al., 2019).

The theory behind AM components with unfused internal pockets is that the motion of densely packed powder within the internal pockets provides inherent damping. Dense packing during the LPBF process is achieved by using a recoater arm to fill the internal geometry of the part with powder and fusing the cavity shut; powder is not optimally placed nor forcefully packed into the cavity. Previous results validating the damping capability of the unfused powder pocket is shown in Figure 7 (Scott-Emuakpor O. , et al., 2018). The four types of specimens assessed were 3.2-mm-thick beams with different pocket locations and/or quantities (Scott-Emuakpor O. , et al., 2018). The unfused pocket size is 17 mm square by 0.65 mm thick, and the four types of beams (all LPBF IN 718) demonstrated the ability to suppress vibration amplitude by as much as 90% (Calculated by the percent difference between solid and minimum pocket Q values) compared to fully fused (solid) beams, data shown in Figure 7. A second study with five types of beams, twice the overall beam and unfused powder pocket thicknesses of the beam, demonstrated strong damping capability as well (Scott-Emuakpor O. , et al., 2018; Scott-Emuakpor O. , George, Runyon, & O'Hara, 2018) Table 1 & Table 2 show vibration suppression as much as 93% in the second study, and the damping capability

can be attributed to less than 3% volume of unfused powder compared to overall beam volume (Scott-Emuakpor O. , et al., 2018; Scott-Emuakpor O. , George, Runyon, & O'Hara, 2018).

Table 1: Damping Comparison of Beams at Second Bending Mode (~250 με) **(Scott-Emuakpor O. , et al., 2019)**

Specimen	Q
Beam 3	411
Beam 2	172
Fully Fused	831

Table 2: Damping Comparison of Beams at Second Bending Mode (~100 με) **(Scott-Emuakpor O. , et al., 2019)**

Specimen	Q
Beam 1	411
Fully Fused	1360

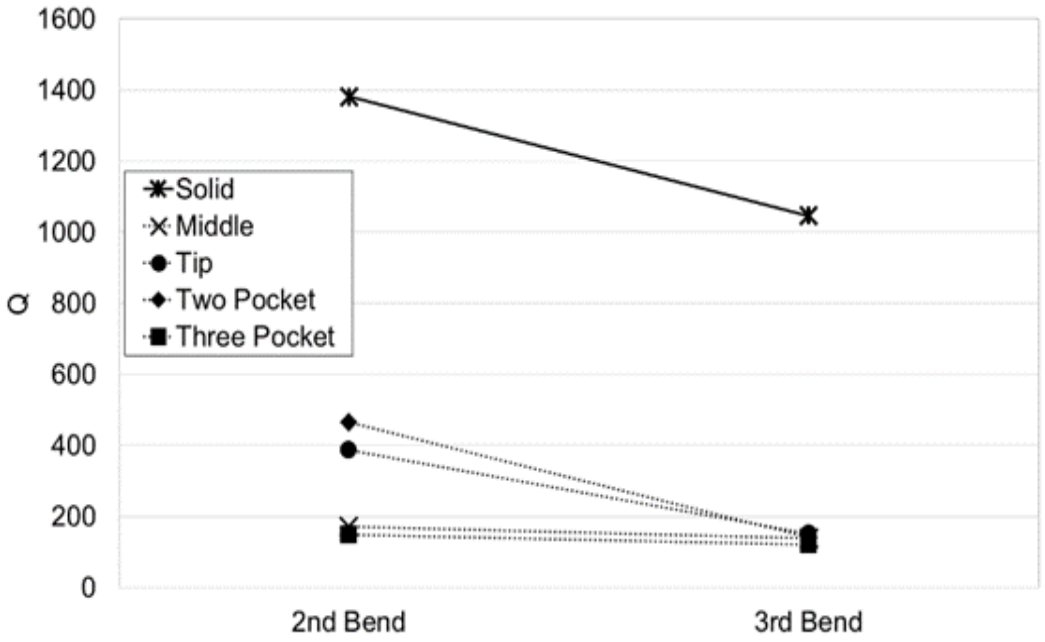

Figure 7: Damping Comparison from Sinusoidal Sweep Tests at Second and Third Bending Modes **(Scott-Emuakpor O. , et al., 2018)**

The strain amplitude vs. damping shown in Figure 8 highlights the loss of damping quality observed in (Scott-Emuakpor O. , et al., 2019). Lower Q values indicate more damping. This shows the loss of damping occurred between the 300 με and 700 με steps.

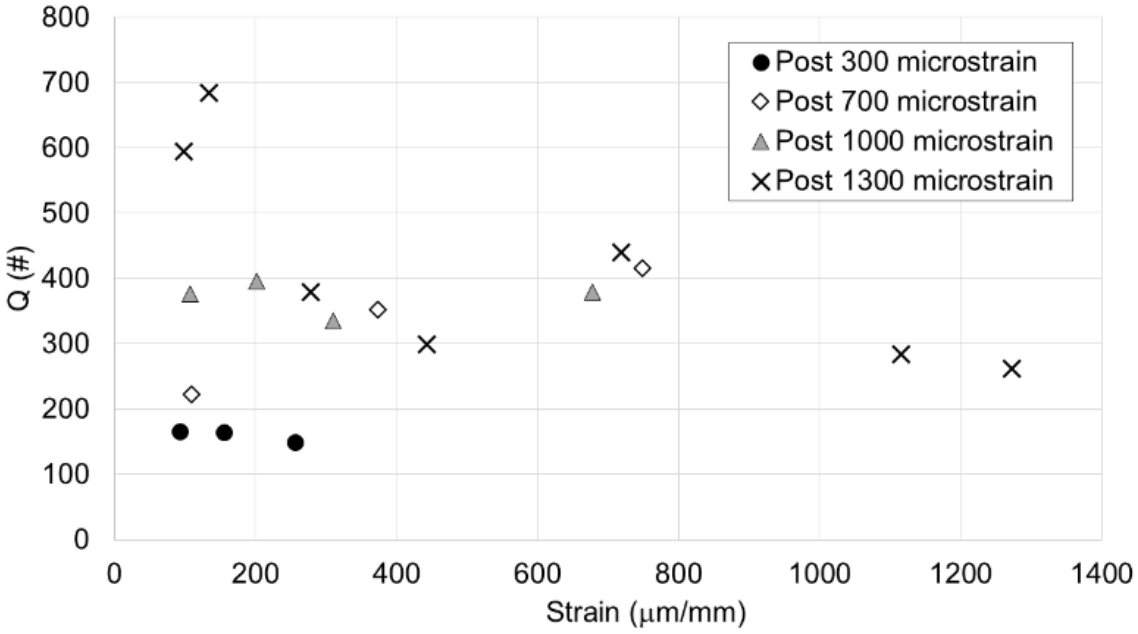

Figure 8: Strain Amplitude from Sinusoidal Sweeps at Second Bending Mode vs. Damping Capability of Two-Pocket Beam **(Scott-Emuakpor O. , et al., 2019)**

TEFF Results on Beam Specimens

With the new method developed by the TEFF of inherent damping using AM (Scott-Emuakpor, George, & Runyon, 2018 Pending) we can take the HCF implication out of the problem thereby limiting life to only LCF implication. This damping technology has been show to increase damping as much as 13X (Scott-Emuakpor O. , et al., 2019). This would mitigate HCF concerns and thus shorten development cycle of gas turbine engines by decreasing type associated with HCF design protocol. It would also allow on demand manufacturing of these engine components.

In prior tests of this technology we have looked into blade pocket location (Scott-Emuakpor O. , et al., 2018; Scott-Emuakpor O. , et al., 2018; Scott-Emuakpor O. , George, Runyon, & O'Hara, 2018; Scott-Emuakpor O. , et al., 2019). It was determined the best location was at the high shear location as the damping behavior operates similar to the opening of a 2nd bend crack. This work will be used as a basis in the placement of the pockets in the blades thus designed herein. The blades will not have optimize pocket placement for this study to keep manufacturing simplified. The next iterations of tests have been focused on evaluating the damping loss mechanism. The TEFF has seen that after bringing the beams up to high strain they have reduced damping capability (Scott-Emuakpor O. , et al., 2019). A series of step test were performed to determine when this would occur and evaluate the strain level that started damping loss. This has shown that at stress level of 700με the damping abilities of the pocket is lower and it is not recoverable. Many methods of recovering the damping have been attempted including random vibration, shock impacting, higher stress vibration, but none have returned the damping quality. These parts have been cut to investigate this behavior and the TEFF team has found that some of the powder seems to be clumped together. This shows that it is likely due to frictional heating causing the powder to fuse thus creating clumps (Scott-Emuakpor o. , George, Runyon, & Sheridan, 3-6 June 2019). This shows the need to check relevancy of this technology to turbine applications as in a turbine you have elevated temperatures and thus this could bring an onset of this behavior.

Different classes of these expendable turbine powered missiles operate at both sub- and supersonic speeds. At supersonic speeds the turbine Fan (1st stage) will see

elevated temperatures at approximately 400°F. This temperature will be used to understand how the pockets behavior when exposed to this environment.

In light of the previous research, the study herein explores the damping capability of uniquely designed LPBF IN 718 blades subjected to high sinusoidal strain amplitude dwells. The purpose is three-fold. First, assess the damping quality achieved in the newly designed pocketed blades with unfused powder. Secondly, explore the endurance of the damping provided by the unfused powder in the pockets. Lastly, assess the structural dynamic changes of the inherently damped blades. The blades were designed by AFRL for structural testing according to openly published design parameters for compressor blades outlined in (Schnoes & Nicke, 2017).

Additive manufacturing is being used in multiple applications in and of the aerospace industry. It has even begun to makes its way into gas turbine engines, mostly in non-rotation parts but in some cases rotating hardware. This shows the applicably of this research topic and how with the combination of multiple research efforts this AM technology of pocketed blades can rapidly applied.

Summary

Multiple technology over the years have attempted to solve the HCF issue. All of the ones discussed above provided adequate damping to resolve the vibratory stress. However all of the methods other than AM add weight and manufacturing complexity to the component. The AM method described above allows for rapid component manufacturing with vibratory stress reduction for use in turbine engines. This method is most immediately applicable to prototyping and unmanned applications like cruise

missile or UAVs, where operational life are shorter and safety margins smaller. This is because of both their single use and limited life as well as the current size of LPBF AM printers.

III. Methodology

Chapter Overview

This chapter lays out the methods which will be used to answer the basic research questions presented in Chapter 1. This chapter discusses initial blade design, blade manufacturing and inspection, experimental methods, endurance test, and all calculations necessary to answer the aforementioned questions.

Blade Sizing Study

In order to test the blades there were a number of design steps that had to be performed including designing the clamp and blades. The blades were designed using some empirical data and following details outlined in Schnoes and Nicke (Schnoes & Nicke, 2017). To produce airfoil data in terms of span, chord and twist dimensions. This data was used to create a blade shape to be used for research that was not designed in an aerodynamic manner but a structurally representative manner. Now with the blade shape determined the next step was to determine the size and to understand AM printability[3] of the pocketed blades. An initial sizing study was performed on two sized blades, one with a 1.35 inch base chord and the other with a 2 inch base chord. They were photographically-scaled to maintain the same mode shapes and scaled frequencies. The main mode of interest for the test was the 2nd bend mode. The blades were then manufactured using LPBF. The 1.35 inch was tested and found to have high damping (Q≈300-450) in the 2nd bend mode and thus would not be a good candidate to study the

[3] Printability referring to the ability to print quality solid blades without performing a build parameters study. Build parameter used were standard for the machine shown in Table 3.

effect of the pockets. Also with the blade being smaller the only other modes that we could capture on the shaker were 1st bend and 1st torsion. The larger blade (2 inch cord) had better damping characteristics with 2nd bend (Q≈1750-2000). This blade also allowed visualization of a 4th mode however, this mode had high damping. The large blade was selected to be printed with a pocket as it allowed a good investigation of the 2nd bend mode and 1st torsion. This difference in damping capability is likely due to using the generic build parameters and could be corrected with a small work effort on build parameter optimization.

Blade Manufacturing and Inspection Blade Sizing Study

The blades were designed as described above and the design is depicted in Figure 9. The blades were manufactured using a Concept Laser M2 Cusing machine with the parameters shown in Table 3. The build plate setup shown in Figure 10, all of the pocket blades and one solid blade were manufactured at the same time and the two other solid blades used in this study were manufactured as part of the initial blade sizing study. There were also two plates one solid and one with a pocket for a different fatigue study. The contour path describes the outer path and the boundary between the skin and the core as seen in Figure 11. Because the pockets must have unfused powder, no heat treating (stress relief or aging) was performed on any of the blades to ensure that the powder remained unfused in the pocket. The clamped surface (platform) was machined to flat and parallel surfaces to ensure the best possible clamping conditions. The designed bolt holes were also final machined.

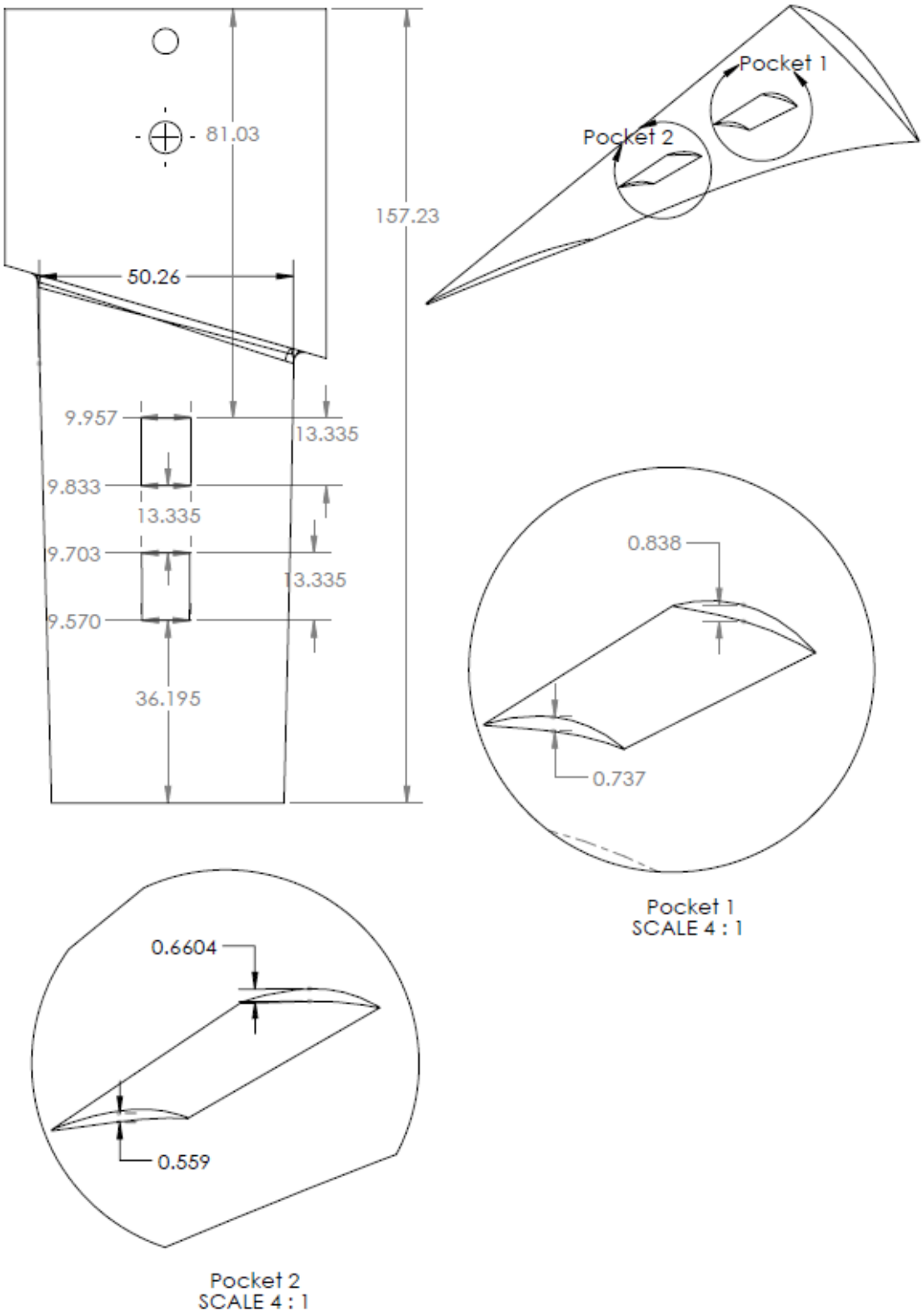

Figure 9: Pocketed Blade Design

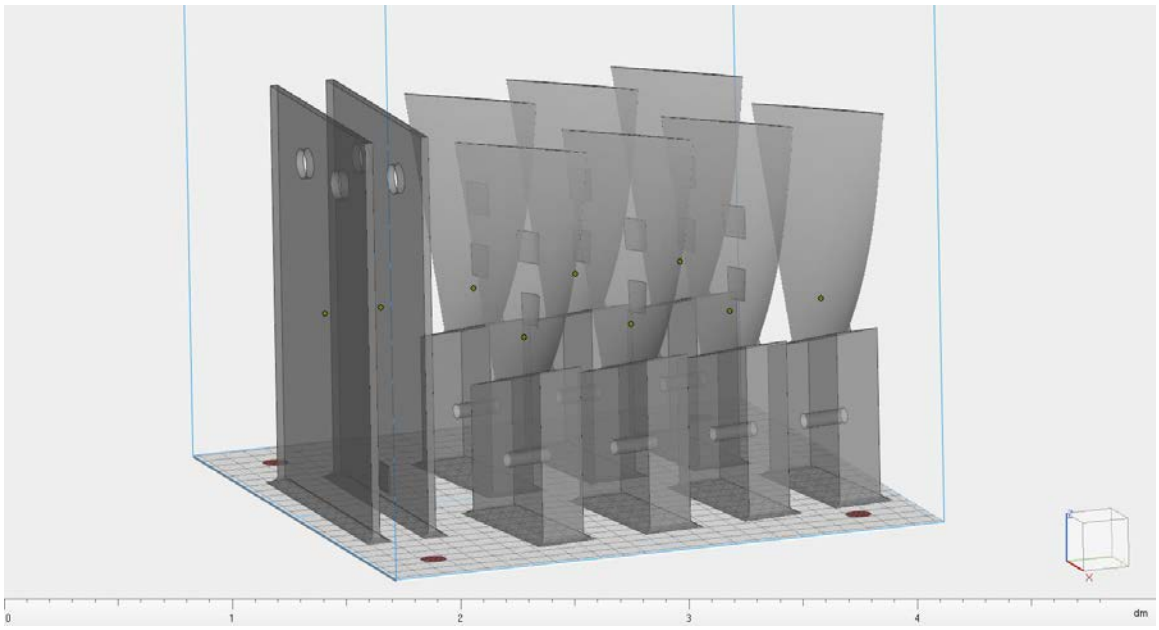

Figure 10: Build plate

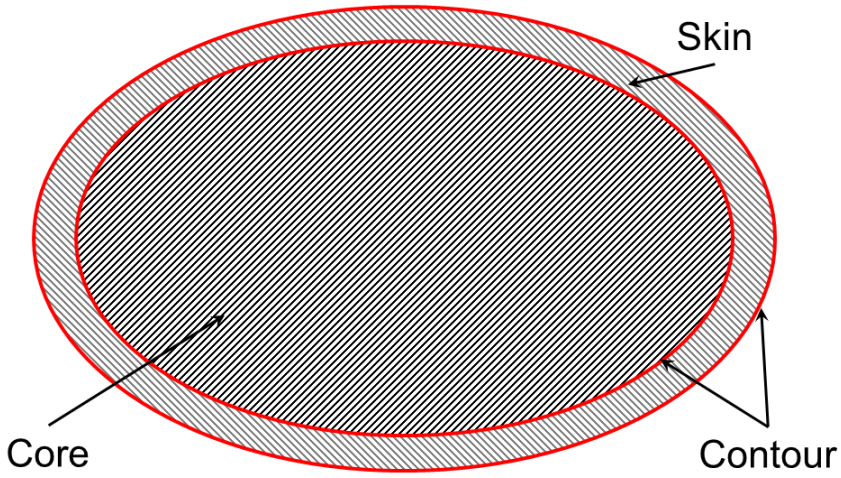

Figure 11: LPBF Build Parameters Description on General Shape

Table 3: LPBF Build Parameters

	Power (W)	Speed (mm/s)	Spot Size (µm)	Hatch Spacing (µm)
Core	370	700	180	130
Skin	180	800	130	105
Contour	120	280	50	N/A

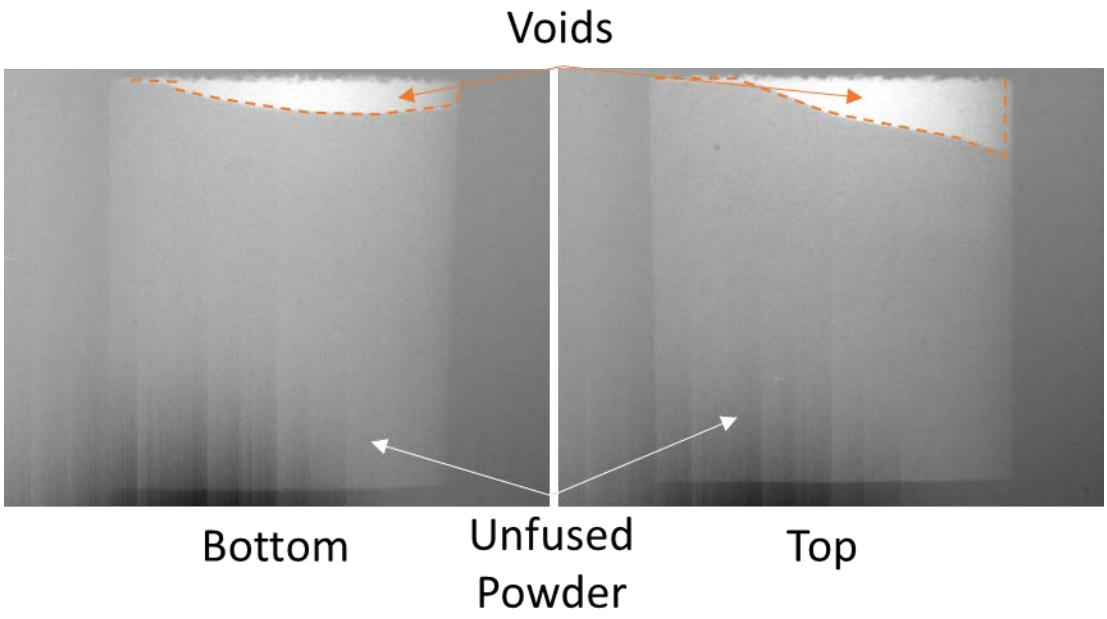

Figure 12: Blade P6 Pocket X-Ray Images

Computed tomography (CT) scans as well as structured blue light scans were performed on the machined specimens to understand the as-manufactured variations in the parts. The CT scans showed variation of the pocket fill, which was calculated and listed in Table 4. X-ray image of two pockets from blade P6 are shown in Figure 12. The pockets were notably less filled than in prior studies. This reduced unfused powder pocket density is likely due to the size, build direction, and complexity of the pockets. The angle of the pocket with respect to the wiper blade direction also could affect this.

Table 4: Void Percentages for Pocketed Blades

Blade	Top or Bottom	Total or Void	Area (Pixels)	% Void	Total Blade % Void	Top Bottom Difference (in % Delta)
P1	Bottom	T	2337984	7.11%	18.55%	4.33
		V	166219			
	Top	T	2282715	11.44%		
		V	261195			
P2	Bottom	T	2094120	8.59%	20.76%	3.58
		V	179874			
	Top	T	2189808	12.17%		
		V	266499			
P3	Bottom	T	2135727	8.31%	19.99%	3.37
		V	177426			
	Top	T	2222550	11.68%		
		V	259626			
P4	Bottom	T	2220048	5.86%	15.59%	3.86
		V	130155			
	Top	T	2285217	9.72%		
		V	222196			
P5	Bottom	T	2092905	7.90%	17.73%	1.93
		V	165399			
	Top	T	2166705	9.83%		
		V	213024			
P6	Bottom	T	2104092	5.95%	14.24%	2.34
		V	125272			
	Top	T	2173824	8.29%		
		V	180215			

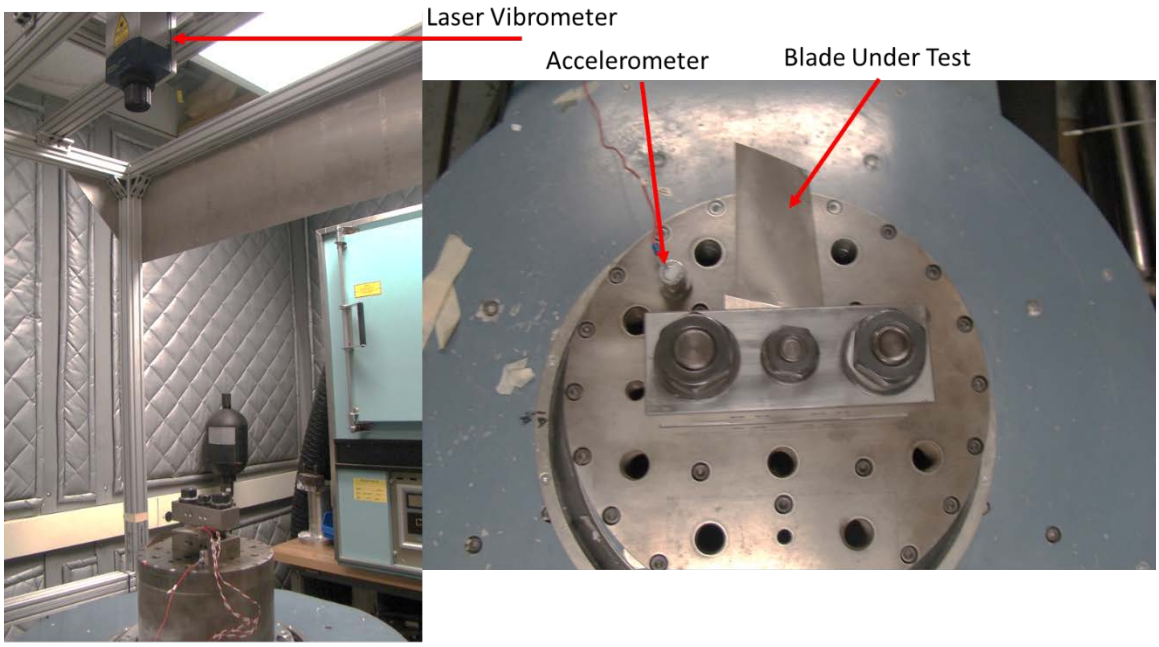

Figure 13: Shaker Test Setup

Experimental Methods

Mode shape analysis allows observations of changes that cannot be seen externally. This study utilized mode shape analysis to determine if changes in the pockets can be measured during operation. This was done by using the Modal Assurance Criteria (MAC) method **(Ewins, 1984)**. The blades were clamped to a 27 kN Unholtz–Dickie electrodynamic shaker head. The force on the clamping blocks was repeated by applying a torque wrench on nuts and bolts (English units used to match hardware and tools used): 120 ft·lb torque on 1-1/16 in. nuts with 5⁄8 in: studs and 100 ft · lb on a 7/8 in. nut with a 3⁄8 in. center stud (see Figure 13). The excitation for the vibration test was supplied by the aforementioned electrodynamic shaker. The Polytec OFV 500 scanning laser vibrometer was used to perform multiple sweeps (sine chirps from x Hz to y Hz) with 3 averages on all scan points. The sweeps were at low amplitude and voltage

controlled by the Polytec system. The scanning points were generated off the FEA analysis of the solid design blade and then imported to the scanning laser using a 3-D alignment. This procedure was repeated for each blade to allow for comparison between each blade as well as the FEA model. The MAC, Equation 1, uses the normalized magnitude of each mode shape in order to compare two measurement sets to determine their similarity. Here σ_r is one vector of points and σ_s the other to be compared. Each of these vectors contains 41 points measured on the blades or extracted from the FEA model. The points were laid out circularly across the blade from the leading-edge tip with higher density near the leading-edge tip and lower near the root. The laser measurement are perpendicular to the shaker head plane.

$$MAC = \frac{\left|{\sigma_r}^t * \sigma_s\right|^2}{({\sigma_r}^t * \sigma_r)({\sigma_s}^t * \sigma_s)} \qquad (1)$$

MAC allows the comparison of mode shape changes from blade to blade as well as a comparison to the FEA model. Based on the placement of the pockets no changes in mode shapes were anticipated.

Damping assessments were made by evaluating results from forced response vibration tests. For this study, forced response tests were conducted on cantilevered LPBF IN 718 blades illustrated in Figure 9. Following the same previously described clamping method, the shaker was controlled with a Vibration Research VR9500 controller. An Endevco 2271A charge-type accelerometer was used to monitor shaker

head acceleration and control the drive voltage. A Polytec OFV 5000 (OFV 505 head) single-point laser vibrometer measured velocity response of the test article at the leading edge tip (long side). The velocity measurement was then correlated to a rosette strain gage, placed at maximum strain location, on the first blade to test. The velocity frequency response from the laser vibrometer was used to assess damping. The data, for each resonance (mode), was captured via swept sine tests at a duration of greater than 30s per half-power bandwidth for a total test frequency range spanning at least three bandwidths. Damping is then calculated as the quality factor (Q) via the half-power bandwidth method (American Soc. for Testing and Materials International, 2017) (Equation 2 & Figure 14). Q originates from the field of electrical engineering and it is the inverse of loss factor, Equation 3, and can be related to the ζ, damping term of a damped oscillator.

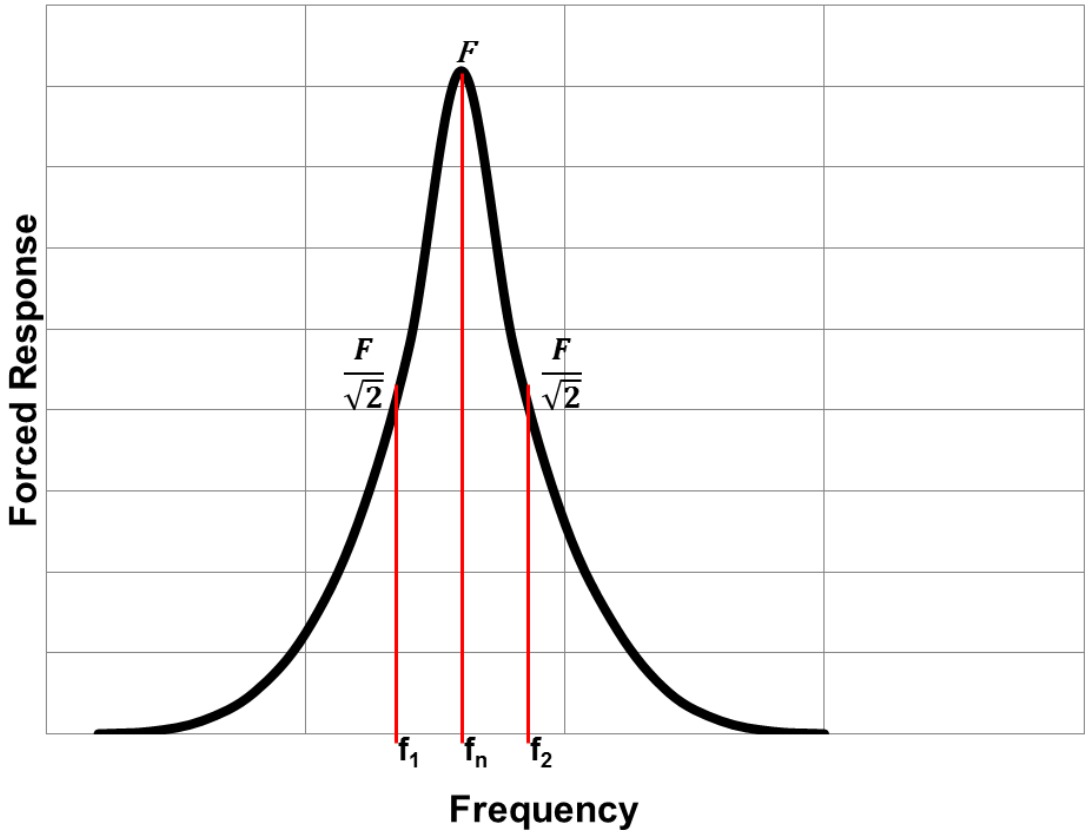

Figure 14: Damping (Q) Diagram

$$Q = \frac{f_n}{f_2 - f_1} \quad (2)$$

$$Q = \frac{1}{\eta} = \frac{1}{2\zeta} \quad (3)$$

Table 5: Comparison of Q Calculation Methods Results for Pocketed Beam

		Velocity Manual	Transmissibility Programmed	
Mode	Accel (g)	Q	Q	%Δ
3	1	50.71	50.90	0.37
3	2	52.31	52.30	0.02
3	3	54.81	54.80	0.01
3	5	63.73	63.70	0.05
2	0.25	117.09	119.00	1.60
2	0.5	119.92	120.70	0.65
2	1	125.26	126.00	0.59
1	0.025	535.41	565.80	5.37
1	0.025	561.77	603.50	6.91

Damping was measured using software which calculates damping (Q) using the half-power bandwidth method off the transmissibility graph. The transmissibility is a measure of the ratio between the laser velocity reading (converted into acceleration) and the base excitation acceleration. This accounts for any changes in base excitation. This is important as the half-power bandwidth omits the effect of control acceleration inconsistencies. This is because the half-power bandwidth method is developed for simple 2nd order peaks and not practical systems, which must take into account changes in input during the sweep. Thus, using transmissibility allows damping performance to be determined with minimal error when compared with the traditional manual velocity peak measurement. This error was studied on a pocketed beam and is shown in Table 5. The two methods are very similar with the exception of mode 1 data. This is likely due to two things, first the low amplitude (Accel=base excitation) of the tests, and second, the

control issues with maintaining constant acceleration with high amounts of motion in first bend.

As stated in the Introduction, the purpose of this study was to observe the damping behavior of the blade geometry in Figure 9 after subjecting the specimen to sinusoidal amplitude dwells at different strain amplitude levels (endurance testing). The duration for each dwell amplitude was controlled to 5×10^5 cycles at the 2nd bend frequency (~1400 Hz). This cycle count was based on prior work and deemed sufficiently high and effect use of test time. The cycles along with the maximum dwell amplitude (600 με) were selected to be in kind with prior work (Scott-Emuakpor O. , et al., 2019) as well as initial findings in this study. The strain amplitude was set in the control system by controlling to a specific leading edge tip velocity (long edge). This was correlated to strain by using a rosette gage on the first blade to determine max principal strain (measured) and its correlation to leading edge tip velocity reading by the laser vibrometer (LV). This was done using a delta rosette strain gage placed on at the maximum strain location from the model (root). The strain dwell tests were performed with two different step sizes. One with steps of 50 με and the other with steps of 100 με.

Endurance Test Setup

The endurance tests were run on the aforementioned shaker. A single point laser vibrometer was used to measure velocity at the leading edge tip of the blade. The first task to complete is to correlate the velocity measured with the maximum strain on the blade. The location of the strain gage was based on the FEA model of the solid blade and based on finding in the MAC data was shown to be true to the pocketed blades. The FEA

stress plot for 2nd bend is shown in Figure 15 and the rosette strain gage was placed at the maximum strain location with the middle rosette perpendicular to the root. Multiple sweeps were performed at increasing drive amplitude (base excitation).

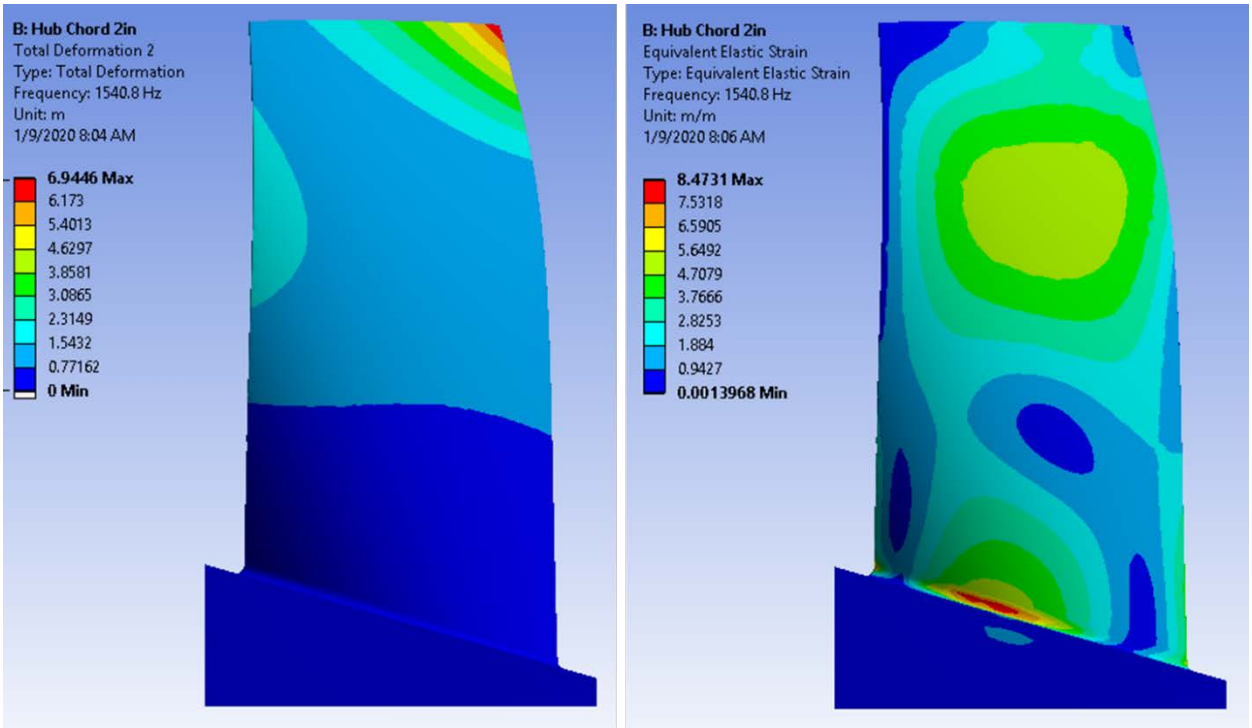

Figure 15: (Left) Mode Shape 2nd Bend (right) Equivalent Elastic Strain 2nd Bend

This data is shown in Table 6 and an example sweep is shown in Figure 16, the maximum principal strain was calculated, using Equation 4 (Micro Measurements, 2014). The maximum principal strain is plotted against the LV measurement and a linear curve fit is made to create the LV to strain equations as seen in Figure 17. Next the endurance test matrix was created by calculating, using Equation 5, the vibrometer reading necessary for the strain steps, shown in Table 7. This was linear for all measurements and is assumed to be linear for this set of tests.

$$\frac{\varepsilon_1+\varepsilon_2+\varepsilon_3}{3} + \frac{\sqrt{2}}{3} * \sqrt{(\varepsilon_1 - \varepsilon_2)^2 + (\varepsilon_2 - \varepsilon_3)^2 + (\varepsilon_3 - \varepsilon_1)^2}$$

(4)

Table 6: Strain Relationship Development

Base Excitation (g)	LV Measurement (mm/s)	Gage 1 (με)	Gage 2 (με)	Gage 3 (με)	Maximum Principal Strain (με)
0.1	86.2	3.3	11.8	7.2	12.4
0.2	157.5	6.9	22.1	13.2	22.9
0.4	306.6	13.3	43.1	25.7	44.6
0.6	443.9	19.1	62.4	37.3	64.7
0.8	590.1	25.1	82.5	49.2	85.5

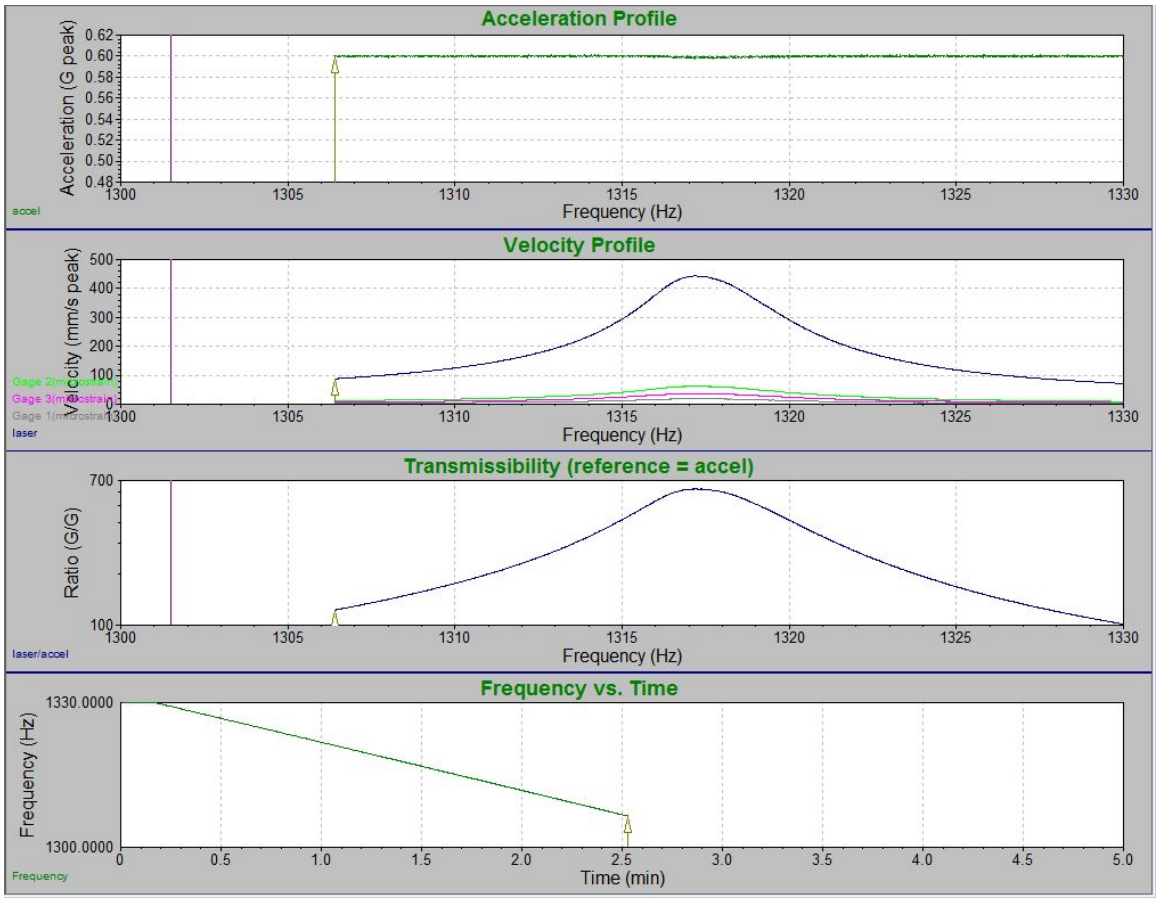

Figure 16: Example Strain Relationship Sweep

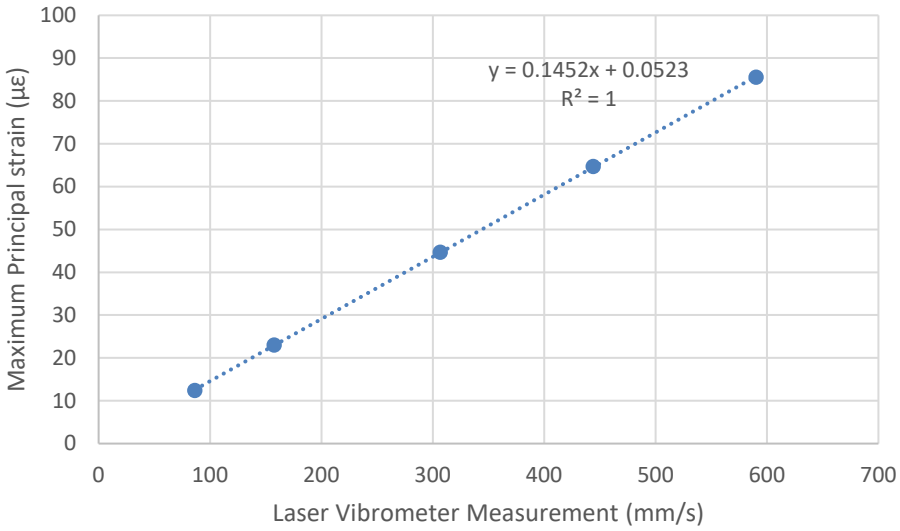

Figure 17: Laser to Strain Relationship

$$Strain = .1452 * LV\_Measurement + .0523 \quad (5)$$

Table 7: Velocity Setting Calculation

Desired με	Velocity Control Setting mm/s
10	69
50	344
100	688
150	1033
200	1377
250	1721
300	2066
350	2410
400	2754
450	3099
500	3443
550	3788
600	4132

The text matrix for each blade can now be created. The same test steps will be followed for each blade and each strain step. The test matrix for all looked like this:

1. Low energy sweep to find 2nd bend frequency
2. Zoom in to create 30hz sweep over 3 minutes
3. Endurance tests
    a. Strain dwell for 5*10^5 cycles (take steady head acceleration measurement, Note dwell frequency)
    b. .1g sweep
    c. .45g sweep (take Q measurement, Maximum velocity measurement)
        i. .45g was selected as the Q measurement sweep due to initial strain measurements of damped blades placing strain level near 50 με
4. Repeat a-c for each strain step (50με or 100με steps) up to 600με

This was repeated for each blade with blades P1, P3, P6, S1 at 50με steps and P2, P4, P5, S2, S3 at 100 με steps. Using two strain step sizes was chosen both for test time as well as cycle accumulation.

Elevated Temperature Endurance Test Setup

The elevated temperature testing was done on the same shaker as the room temperature testing. A thermal insulator was used to protect the shaker head from the high temperature, and is shown in Figure 18. A heated box called a 'hot box' was used to encapsulate the blade under test. This hot box has a heater and air temperature

thermocouple built in for heating and control. In addition, two cartridge heaters were used by placing them in the bottom clamping block in pre made holes. The cartridge heaters were controlled by a thermocouple attached to the bottom clamping block. For the test setup, blade S1 was used to understand temperature profile (This test was performed after the room temperature testing and thus did not affect its data). Four thermocouples were spot welded to the blade center line from tip to root seen in Figure 19. These measurements allow us to understand blade metal temperature. After installing the blade an optical path was created to allow vibration measurement.

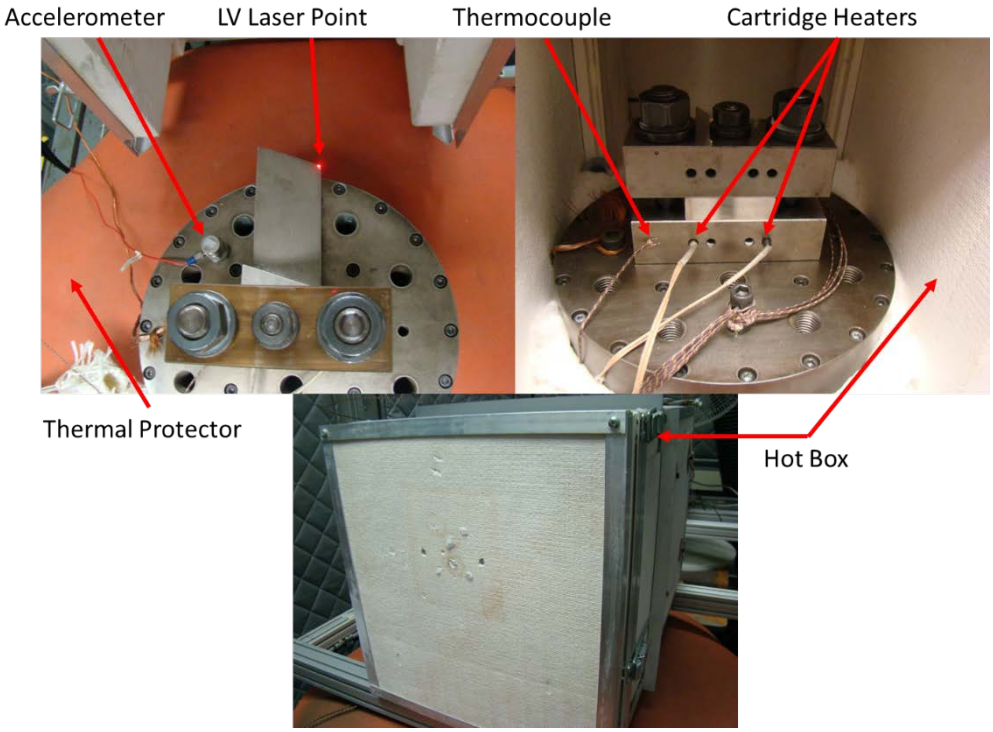

Figure 18: Hot Box Setup

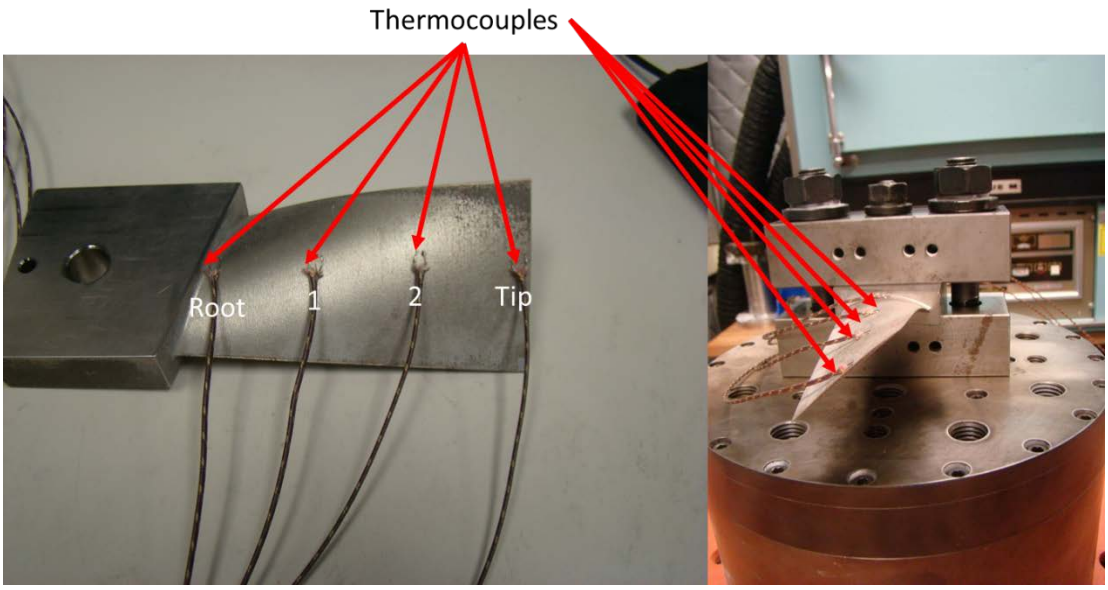

Figure 19: Thermal Blade Setup

Blade S1 was used to understand the necessary set points for the oven and soak time to achieve blade temperature. The set points selected after this testing were 405°F for the air heater and 350°F for the cartridge heater. This was selected both based on achieving the desired 400°F blade temperature and time as the cartridge heaters were very slow in heating the block. The soak profile is shown in Figure 20. This shows that the blade tip was very close to the air temperature and a slight cooling effect for the root due to heat loss through the block. The likely reason the root was hotter to start is that the cartridge heaters working at constant on vs. duty cycling once set temperature was reached. This was because the air temperature was able to reach its set point quicker than the block. The time span of thermal soak was selected at 35 minutes. Temperature data was then taken for 2 hours so that we can understand the temperature change that will be seen through the strain testing which takes ~2 hours per blade.

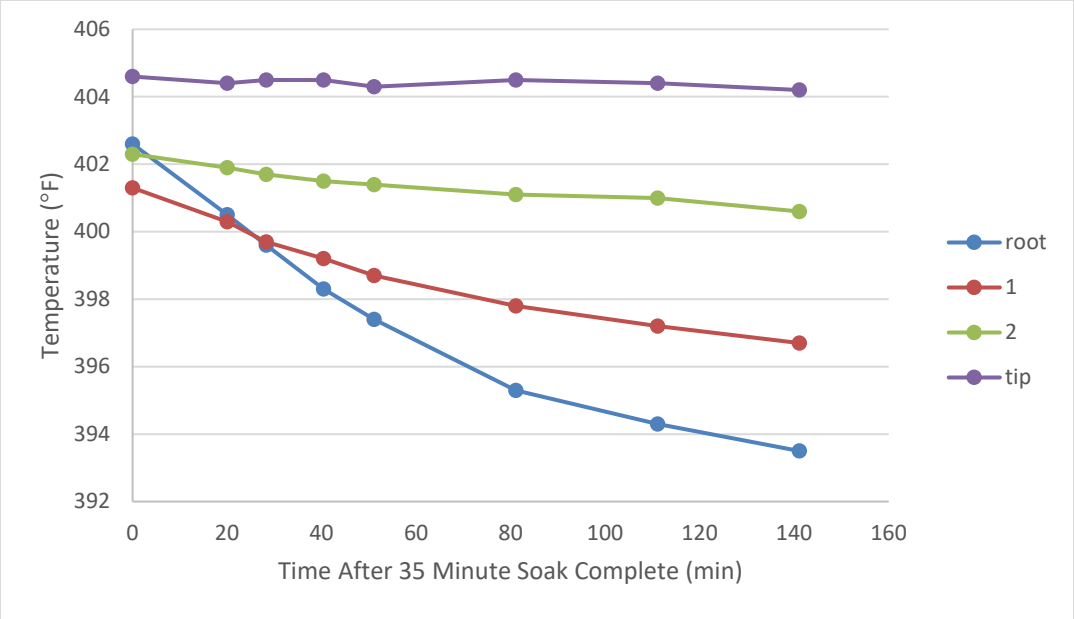

Figure 20: Temperature Soak Profile

This setup was used in all elevated temperature endurance testing discussed in the following chapter. This setup ensures that the blade is within the 400°F range during the entire test profile.

Summary

This chapter outlined the methods undertaken to study and answer the questions outlined in Chapter 1. These methods allowed for an understanding of the inherent damping of AM when applied to a turbine engine blade design. The results of these tests will be discussed in the next chapter.

IV. Analysis and Results

Chapter Overview

The damping performance, strain limitations, and the influence of temperature of the manufactured gas turbine engine blades, with and without pockets, is analyzed and compared using the methodologies presented in Chapter 3. These tests were conducted at the TEFF, Wright-Patterson AFB OH under the guidance and tutelage of the government civilians and contractors there. The tests founds that the blades had similar performance to the beams mentioned in Chapter 2. The elevated temperature testing showed similar results in general with slight difference in end state of the pocketed blades.

Results Pre-Endurance Inspection

Top vs. bottom pockets were analyzed by the percent of void area/volume with respect to the total area of the pocket as measured by CT images. Comparison of top and bottom pocket void percentage is presented in Figure 21 in the form of a boxplot. This boxplot of the sampled top pocket fills vs. bottom fills strongly suggests that the median of the top pocket fills is greater than the bottom pocket fill by 3.24%. This was likely caused by the angle of the pockets due to the blade's twist as the fused material grows with respect to the recoater arm. No evidence was found to correlate pocket fill and build plate location and all of the pocketed blades were on the same build plate.

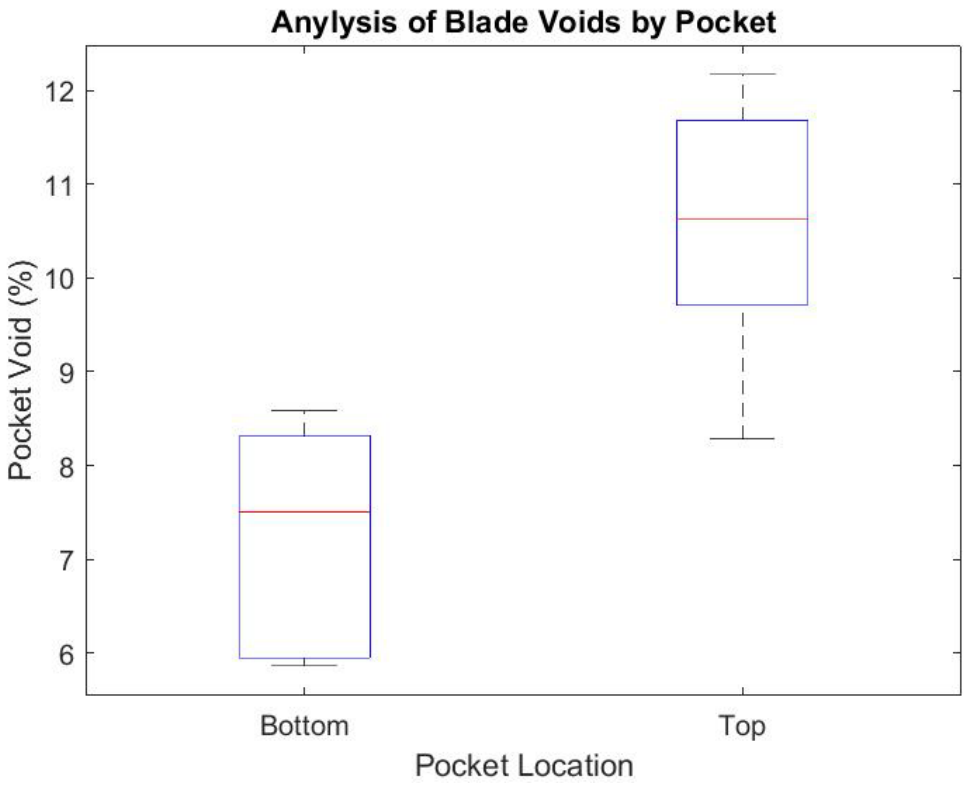

Figure 21: Boxplot of Void Percent and Pocket Location

Structured light scans were performed on each of the blades and then the external geometry was compared to the designed geometry to determine variations, these measurement are shown in 'heat plots' as seen in Figure 22. This study found that blades P1, P2, and S2 were warped by a maximum of ~600 μm at the leading edge tip with the others having only slight deviations (<300 μm) from nominal. Blade P2 is shown in Figure 22, where the twist is shown by the red (extra material) on the pressure side and the blue (less material) on the suction side depicting twisting of the blade along the leading edge. The platform color is unimportant as it was machined to flat and parallel. The exact width of the platform (grip section) has no bearing on the test results. This is

because the platform is all under the grip section and thus does not affect the vibratory response of the blade as long as it is flat and parallel for clamping.

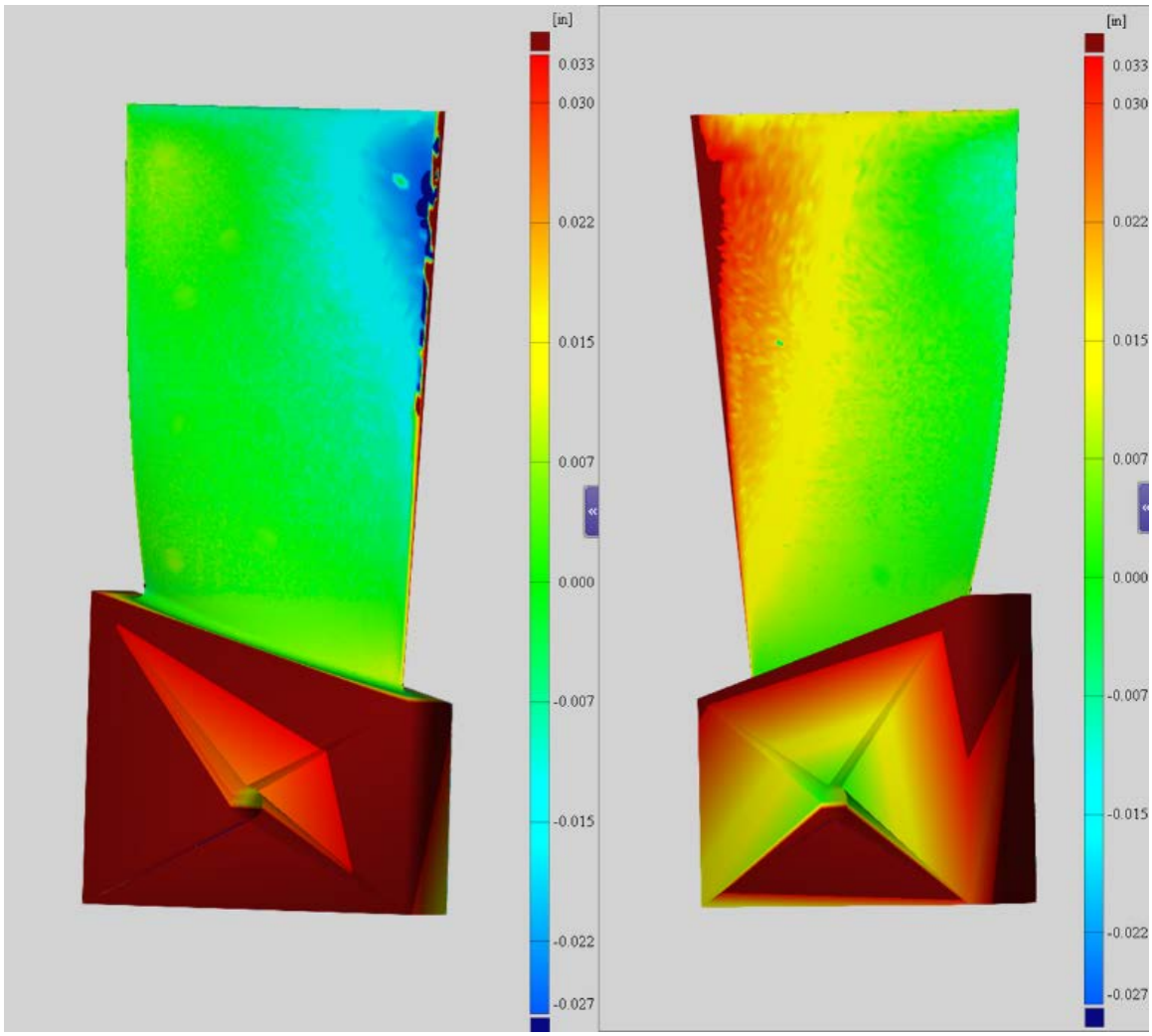

Figure 22: Structured Light of Blade P2. (Suction Side Left, Pressure Side Right)

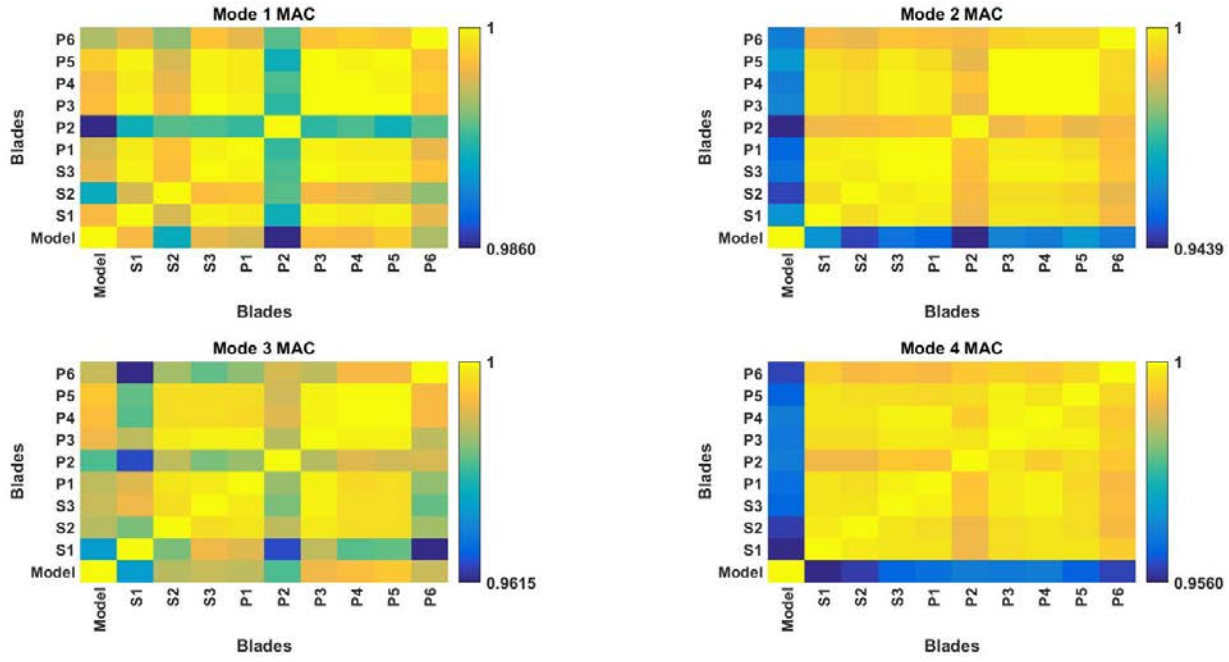

Figure 23: Pre-Endurance Testing MAC Study between Model and 9 Blades for Modes 1-4 (Ambient Lab Conditions)

A MAC analysis, shown in Figure 23, was performed to investigate variation of the mode shape/modal response between the model, the solid blades, and the pocketed blades pre-endurance testing. The associated frequency variation is shown in Table 8. The pre-endurance testing MAC shows at least 94.4% mode shape agreement. The deviation of less than 5.6% is typical and consistent with published work (Naik, Lehmayr, Homeier, Klaus, & Vogt, 2019; D'Souza & Epureanu, 2012; Gillaugh, Kaszynski, Brown, Beck, & Slater, 2019) . Therefore, it can be stated that the pockets did not significantly affect the mode shapes. This MAC analysis indicates that the warping, caused by the fabrication process, did not significantly affect mode shapes. This is likely because the warping occurred in an anti-node location for all 4 modes in the same direction as the blade would be deflecting. The frequency variation is at most 7%.

To understand this frequency variation, work must be done to understand the changes to mass and stiffness created by the pockets. The assumed mass and stiffness affected the bending modes (1, 2, & 4) more than the torsional mode (3). The torsional mode (3) is fundamentally different in how it interacts with the clamp and thus frequency was affected differently.

Table 8: Frequency Variations (Hz) Measured From Blade S1 Ambient Lab Conditions

S1 (Hz)	476.6	1418.0	1853.0	3086.0
Variation (Hz)	Mode 1	Mode 2	Mode 3	Mode 4
Model	42.7	121.5	119.1	31.5
S1	0.0	0.0	0.0	0.0
S2	4.4	10.0	2.0	2.0
S3	-35.2	-107	-12	-215
P1	-33.7	-100.0	-15.0	-163.0
P2	-27.9	-83.0	-9.0	-208.0
P3	-16.6	-52	17	-143
P4	-17.1	-59.0	22.0	-158.0
P5	-5.4	-23	58	-112
P6	-0.5	-11.0	50.0	-91.0

Results Pre-Endurance Damping Performance

Next, damping results were measured from sine sweeps with base excitations of 0.45g on all 6 blades. Table 9 shows the initial damping of each of the blades. The results show an 80-83% vibration suppression due to unfused powder pockets. The damping study showed that the pockets proved to damp vibrations slightly lower than found in prior study (Scott-Emuakpor O. , et al., 2018; Scott-Emuakpor O. , George, Runyon, & O'Hara, 2018; Scott-Emuakpor O. , et al., 2019). This initial damping can be viewed in regards to the pocket void percent, Figure 24. This shows a possible

correlation between the fill amount and the initial damping. Pockets with high powder density have better damping performance. Additional tests are required to definitively support the observation as well as determine why the void% varied as much as it did in the manufacturing of these pocketed blades.

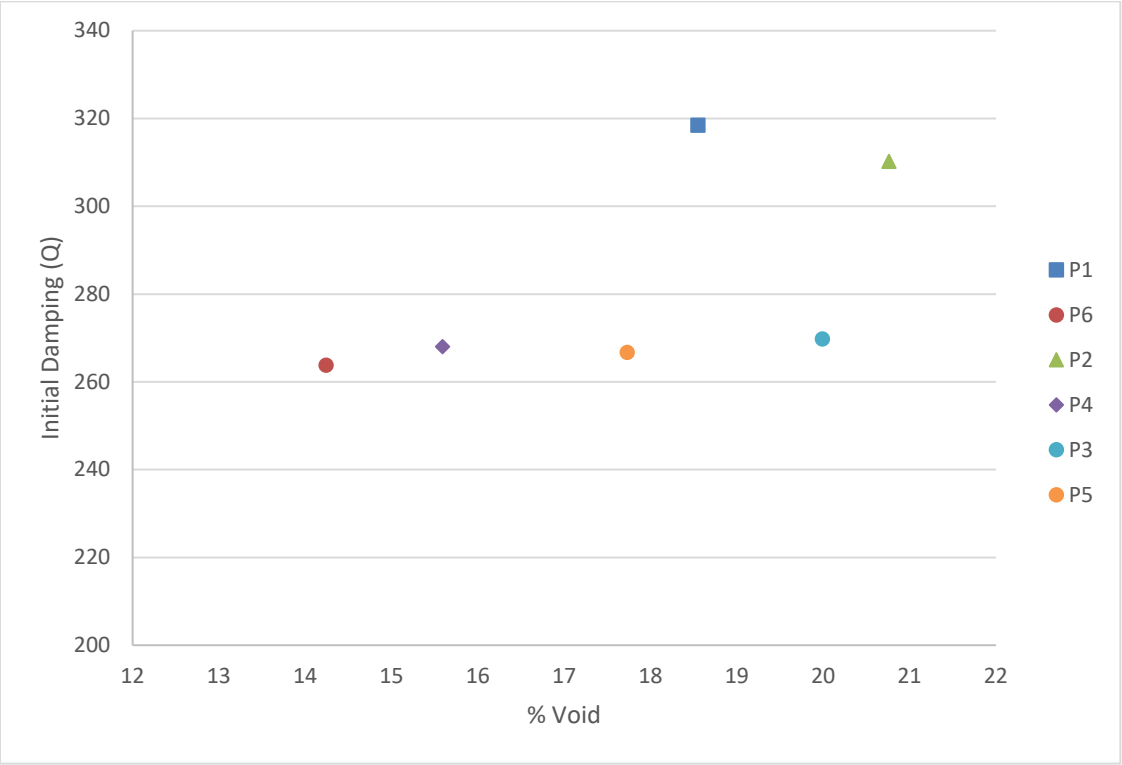

Figure 24: Initial Damping vs. Total Pocket Void % Ambient Lab Conditions

Table 9: Initial Damping Measurements at Constant Base Excitation Ambient Lab Conditions

Blade	Damping (Q)
S1	1596.7
S2	1518.6
S3	743.8
P1	318.5
P2	310.2
P3	269.8
P4	303.0
P5	266.7
P6	297.0

Results Room Temperature Endurance Testing

The endurance testing was performed with two different με step sizes as outlined in Chapter 2. The 50 με step blades are blades P1, P6, & S1 and the 100 με step blades are P2, P4, & S2. The first blade tested and therefore strain gaged was blade P1. A strain gage was placed on the blade to provide a correlation between maximum principal strain and the velocity measured by the laser vibrometer. The damping data is plotted such that the sinusoidal strain amplitude dwell performed prior to sine sweeping and Q calculation on the x-axis, the subsequent damping is on the y-axis, this is shown in Figure 25. This shows that the loss of damping is not immediate but in fact gradually occurs with accumulated damage. It can be seen that the reduced damping has a level at which the maximum reduction is done but it is unclear if that level was reached for all the blades. The tests were cut off at 600 με due to one of the blades (P1) exhibiting behavior indicating a crack. The dynamic response indication is similar to that seen in published vibration fatigue work with a frequency drop of more than .1% during sinusoidal amplitude dwell testing (Scott-Emuakpor, Shen, George, & Cross, 2008; George, Seidt, Shen, Cross, & Nicholas, 2004; Bruns, 2014; Scott-Emuakpor, Sheridan, Runyon, & George, 2020). The crack location has not yet been determined, but it is likely not in the pockets based on observations made by Scott-Emuakpor et al. (Scott-Emuakpor, Sheridan, Runyon, & George, 2020).

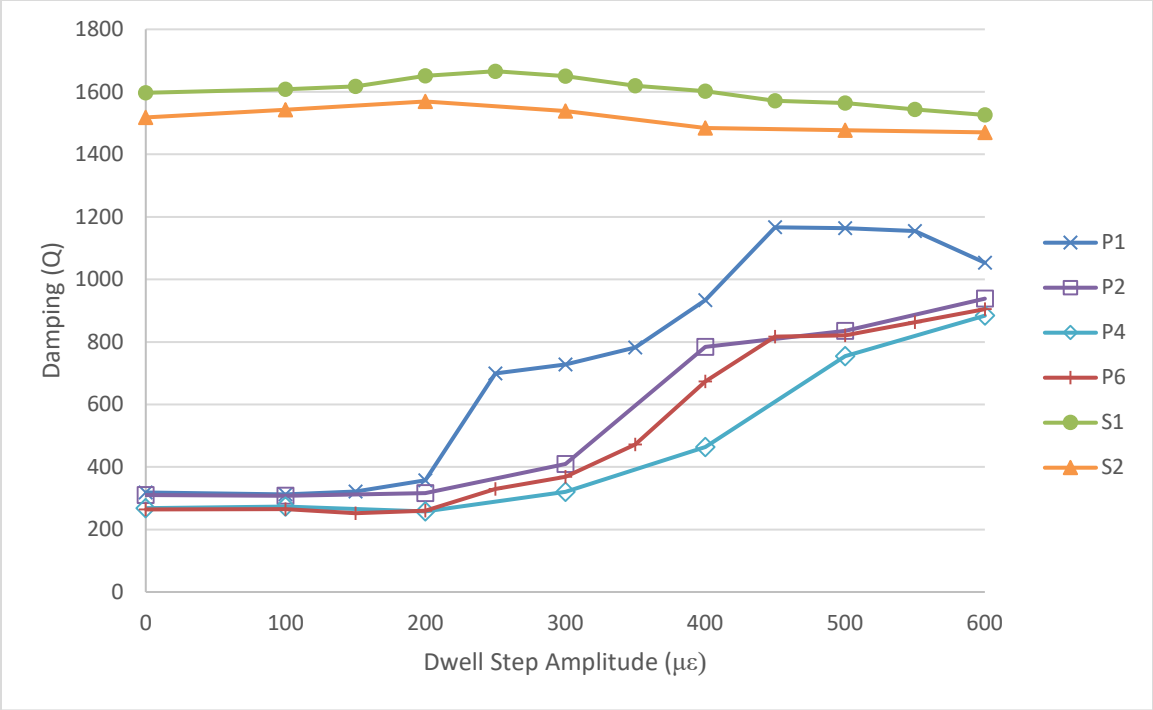

Figure 25: Measured Damping after Sinusoidal Strain Amplitude Dwell Room Temperature

The change in frequency from the initial sinusoidal dwell frequency (Δ) is shown in Figure 26 (mode 2 only). This shows the difference between the frequency change the solid blades (S1 & S2) compared with the frequency change in the pocket blades (P1, P2, P4, & P6). The difference shown show that the changing powder dynamics, due to the loss of damping quality shown in Figure 25, do affect frequency.

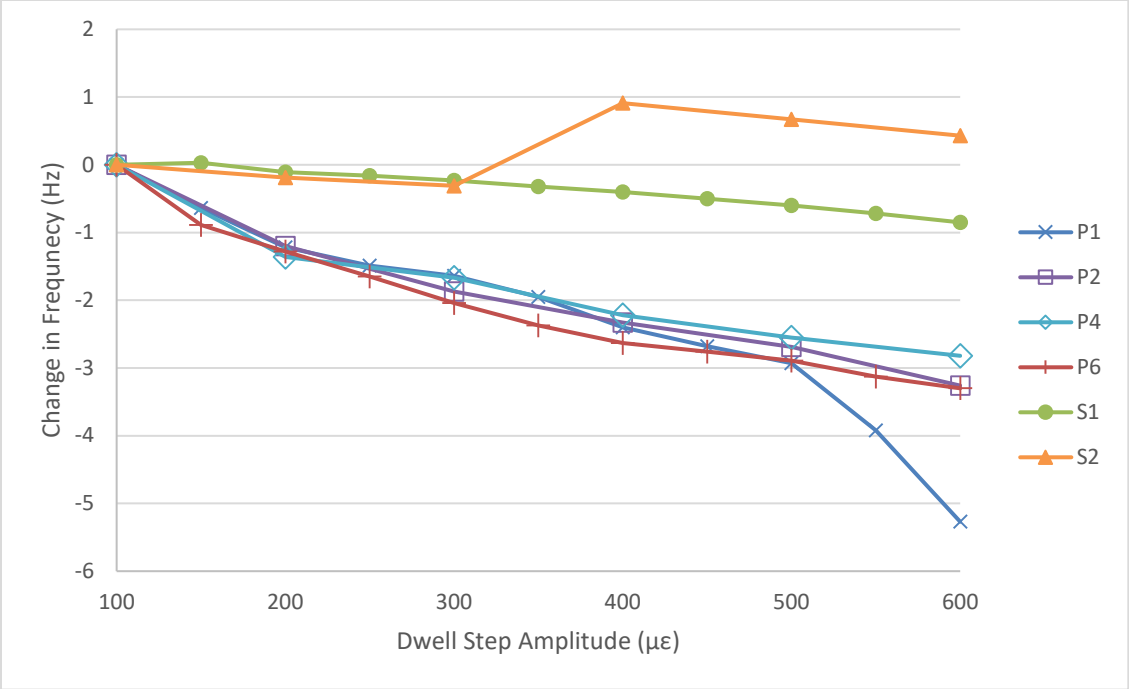

Figure 26: Frequency Change from Initial (100 με) Sinusoidal Strain Amplitude Dwell

Powder Dynamic Notes

It is important to note that the damping achieved by the powder pocket is purely a dynamic phenomenon. When testing at elevated strain level it is common to see oddities (plateau or double peaks) in sweeps. It therefore follows that these oddities are changes in the clamp condition. However in this case, it is believed to be changes in the powder pocket structure. The current theory of pocket lockup states that the powder is fusing together and to the walls. After strain cycle steps the raw vibratory sweep data occasionally suggested an abnormal peak. They are characterized by sweeps that have double peaks or are plateaued peaks. These peaks are impossible to get damping measurement on, and in this study a second sweep is run showed the oddity to not be

repeatable. This is what has led us to characterize this as part of the powder dynamics within the pocket, and it settles after sweeping through.

Results Post Room Temperature Endurance Inspection

The post-endurance testing mode shape comparisons shows similar MACs to those seen pre-endurance testing. This can been seen by comparing the minimum values seen in Figure 23 and Figure 27. This indicates that the reduction in damping does not affect mode shape. This follows since the pocket vs solid blade comparison showed little mode shape difference. The post-endurance testing MAC shows at least 94.1% mode shape agreement with a maximum difference between pre-endurance and post-endurance testing of less than 1.1 %. The variations between the pre-endurance and post-endurance testing mode shape is within expected repeatability of the tests. This is a reasonable conclusion due to pocket size (<1% of total volume) and location (around the neutral axis). Table 10 shows the frequency variation post-endurance testing, this frequency change was measured off the low energy MAC tested performed after the endurance test and comparing them to the same setup before the endurance test. The variation was at most 0.45% on blade P1 which is assumed to be due to the potential crack

Table 10: Post-Endurance Test Frequency Variation (Hz) Room Temperature

Variation (Hz)	Mode 1	Mode 2	Mode 3	Mode 4
S1 Post	0	-2	-3	-11
S2 Post	0	1	-1	4
S3 Post	-4.4	-25	0	-89
P1 Post	-1	-6	-3	-10
P2 Post	-0.5	-2	-3	-5
P3 Post	0	-4	-2	-39
P4 Post	-0.5	-1	-3	6
P5 Post	0	-4	-2	-36
P6 Post	0.5	-1	-1	-6

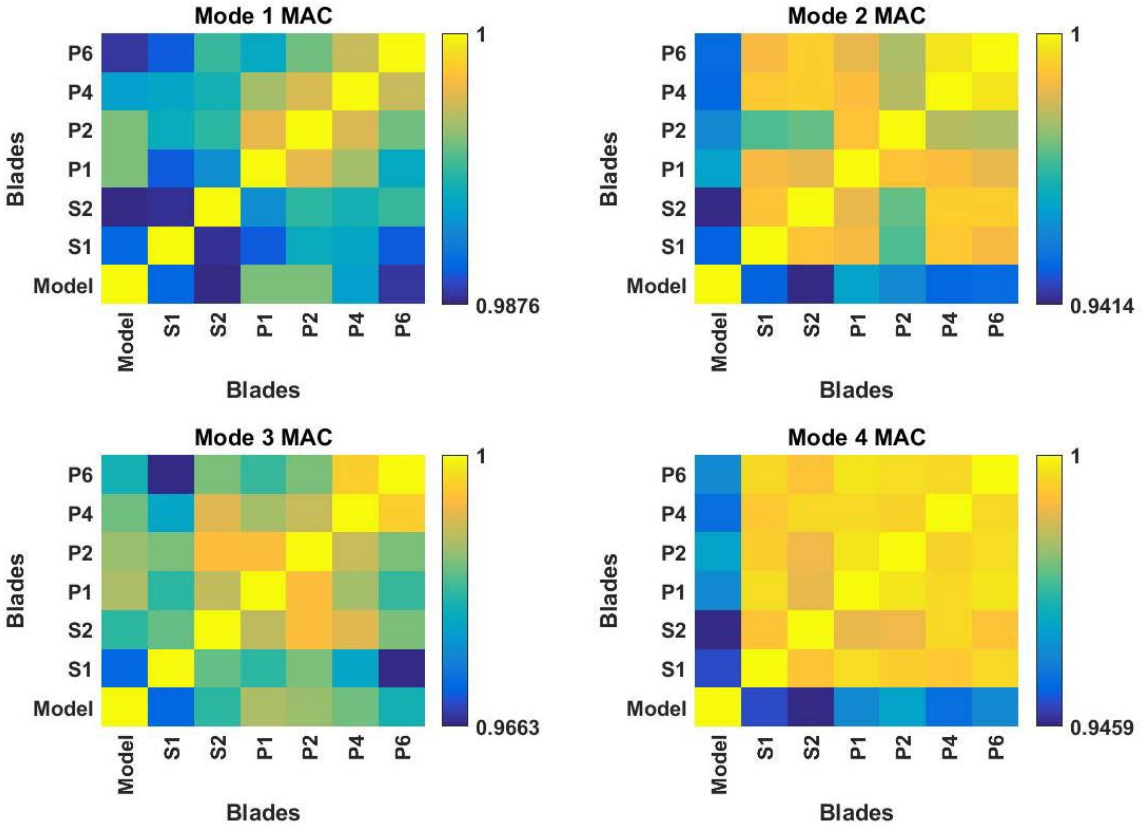

Figure 27: Post Room Temperature Endurance Testing MAC Study between Model and 6 Blades for Modes 1-4

At the final strain step (600 με) it was found that it took an average of 1.45 times the energy (input base excitation) required to achieve a given strain value. This is similar to previous results and demonstrates that even after the blades have lost most of their damping they still have better damping than the solid blades. This finding encourages further application research anywhere AM can be applied and vibration reduction is required or helpful.

After all blades completed experimental testing a post X-Ray image was taken, as seen in (Figure 28) , to provide insight into the powder pocket changes. A definite change can be seen when Figure 28 is compared with Figure 12. The density changes shown in Figure 28 are assumed to be correlated to the loss of damping mechanism. This mechanism needs further study but could be related to heat generation and change in the powder structure. The local density changes observed show a change in the powder structure from free powder to locally fused and affixed to the walls. Additional destructive and non-destructive tests will need be performed to evaluate unfused power condition outside of this work effort. All of the other blades showed similar results with some still showing signs of having some free powder.

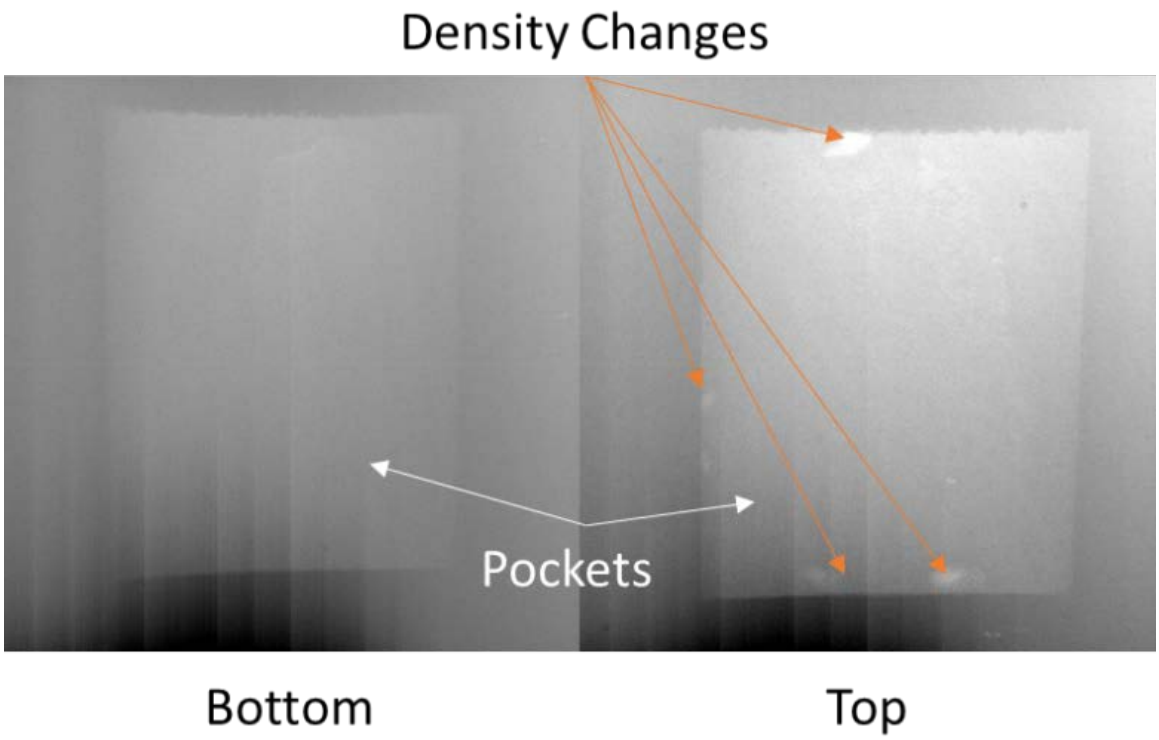

Figure 28: Blade P6 X-Ray Images Post Room Temperature Endurance Test

The tests herein show the utility of this technology. The novel use of unfused powder in LPBF AM allowing for weight reduction, and force response reduction provided a powerful argument for application. The negligible effect on mode shapes and slight effect on frequencies allows for modification of existing AM design with limited engineering changes. Additionally, it makes a strong statement to leverage AM design methods.

Results Post Elevated Temperature Endurance Testing

Temperature data was collected inside the oven by use of thermocouples. The first blade (S1) had multiple thermocouples along the length of the blade in order to understand how the blade was heating and come up with a settling time. After the initial

thermal soak, the temperature profile was determined, as described in Chapter 3, to be a 35 minute thermal soak. This was used for the 3 blades.

It is noted that the pockets could have an effect on the heating of the blade under test. This was discussed by the experts at the TEFF and it was decided that based on the thermal profile from the solid blade that the pocket would not change the heat soak profile. There will however be heat generation in the pocket once strain endurance testing begins this has been seen in prior testing to be around a heat generation of 1ºF.

The elevated temperature damping endurance data was analyzed in the same manner as the previous section. The temperature damping endurance is shown in Figure 29 as well as the frequency change data in Figure 30.

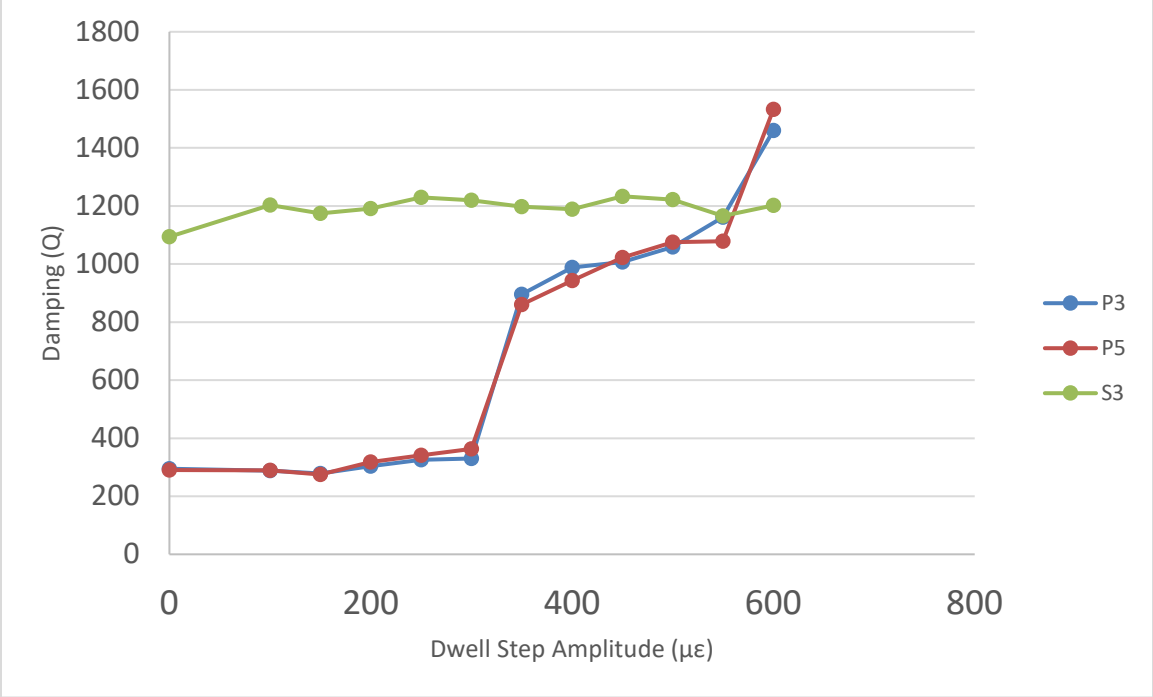

Figure 29: Damping Change after Strain Dwell For Temperature Data 400 °F

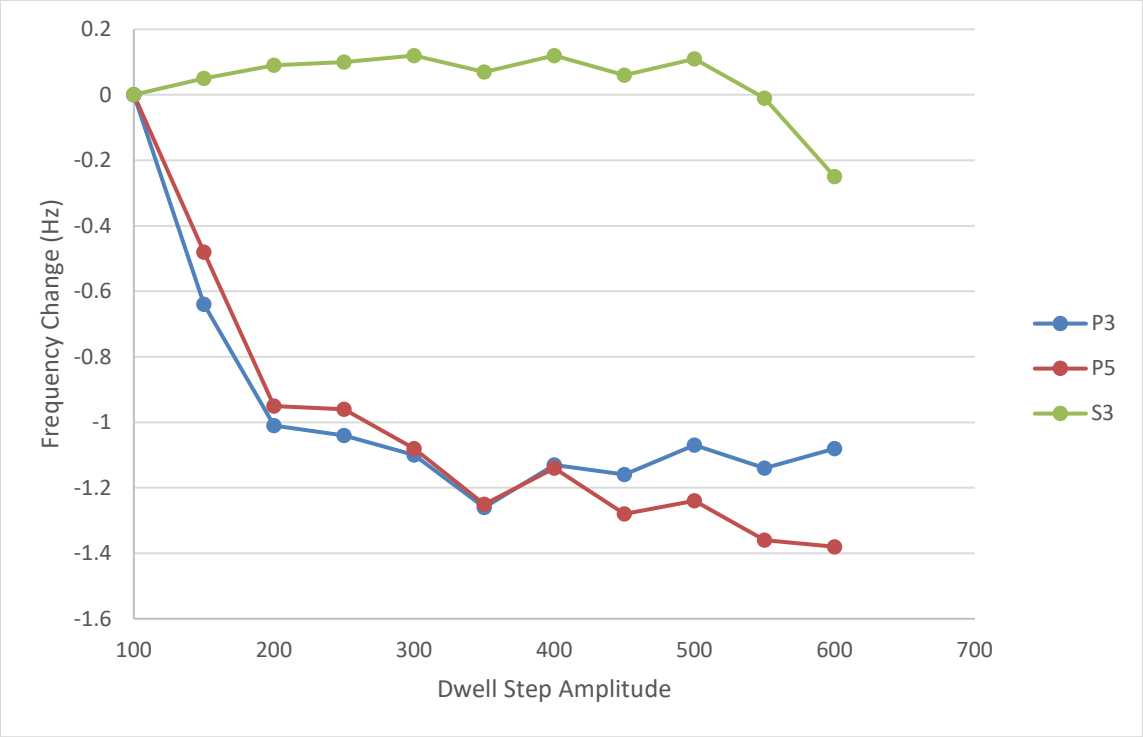

Figure 30: Frequency Change for Temperature Data 400 °F

During testing of S3 two things were of significate note. Initial when comparing initial damping (Q) number S3 was notably more damped (lower Q) then the other two solid blades, this was noted at room temperature and elevated temperate (shown in Table 11). This and when the blade was undergoing endurance testing on the last step (600με) the blade showed a frequency shift that indicated a crack had formed (as see in P1 during room temperature testing).

Table 11: Solid Blade Initial Damping Comparison

Initial Room Temperature	
Blade	Damping (Q)
S1	1596.7
S2	1518.6
S3	743.8

This data can also be shown in relations to the room temperature data. This is shown in Figure 31and Figure 32 (With the temperature data show with dotted lines).

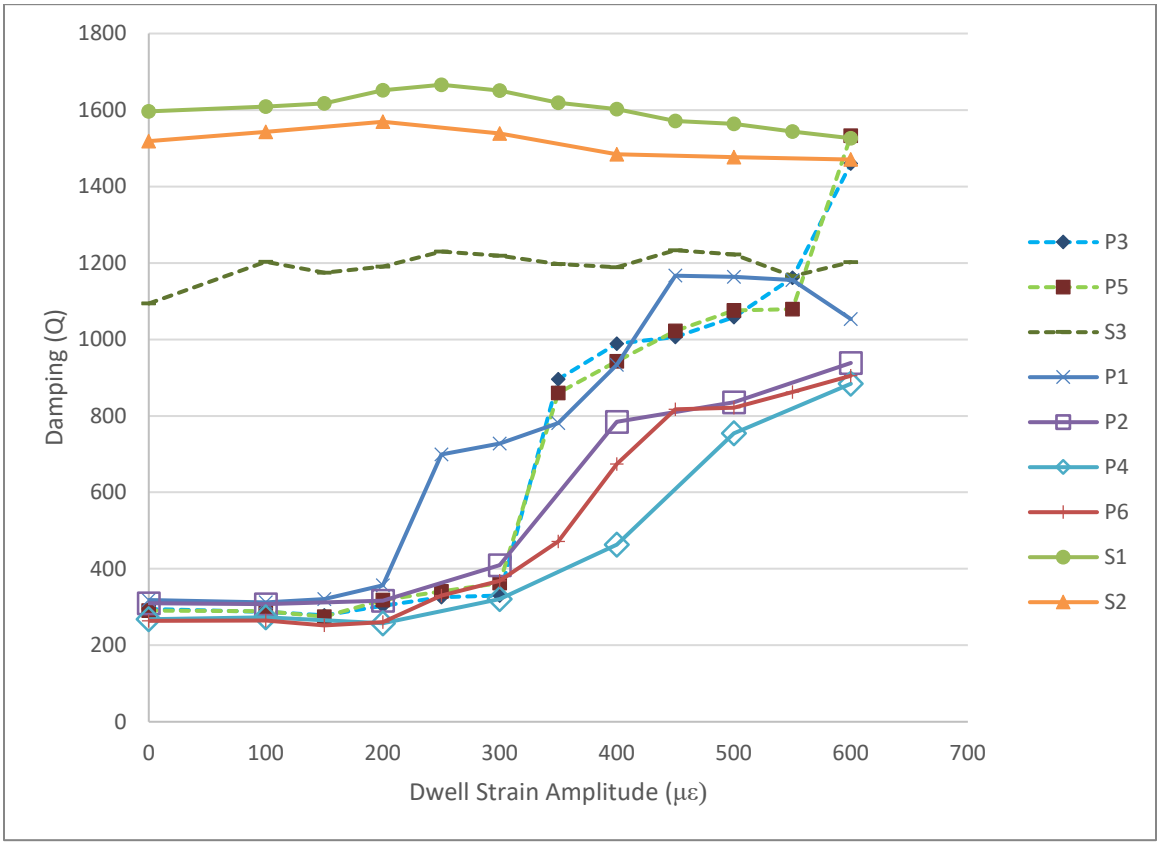

Figure 31: Damping Change All Blades

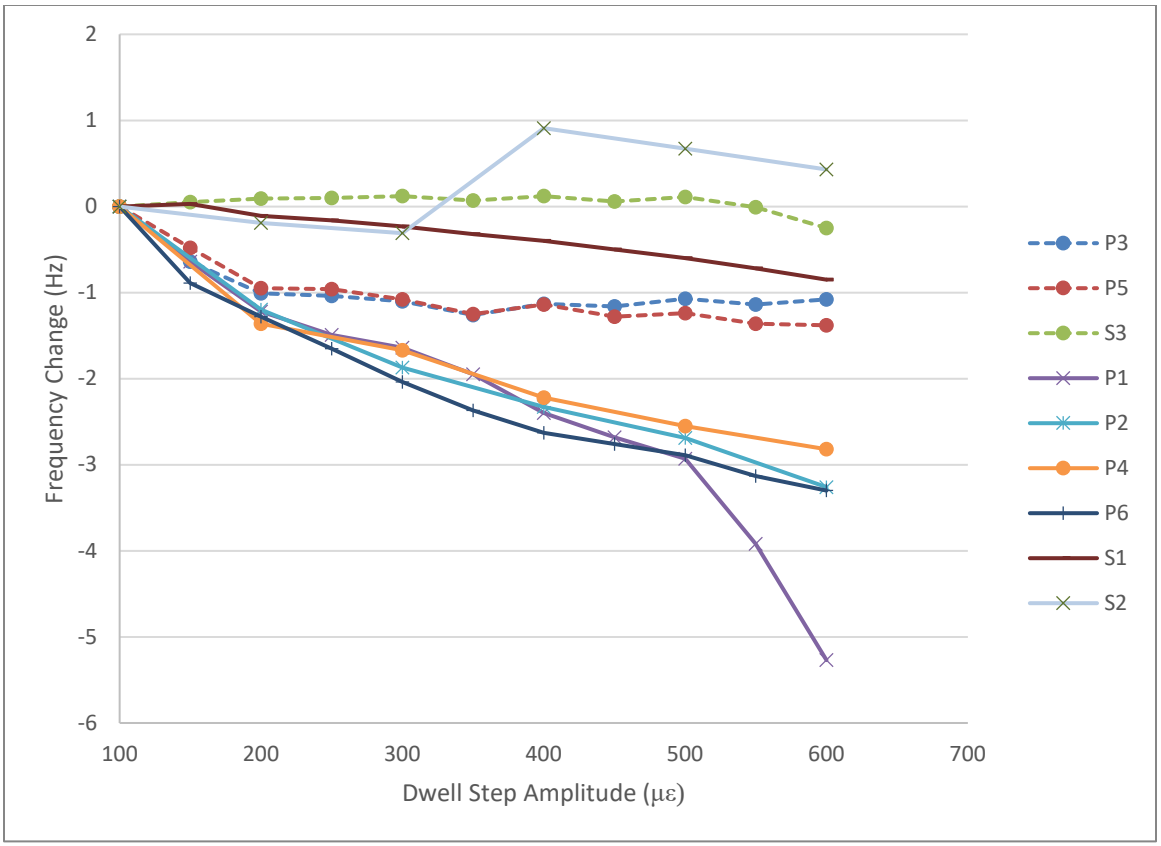

Figure 32: Frequency Change All Blades

The figures above show that there was a difference for endurance testing at elevated temperature. As well as that the final state of the blades was significantly higher Q's. This supports the conclusion that the loss of damping quality is linked to heat and likely heat generation inside the pocket. The large step seen after the 350 με seem to indicate a more specific strain limit at temperature.

This is easier to visualize when viewed as the average temperature damping measurement with P6, show in Figure 33. P6 was chosen, to compare with average temperature blades, since it also was done at 50με steps and had no indications of crack formation that P1 had. P6 also followed the trends shown in the two other pocket blades

tested at room temperature (P4, P2). The average was computed by taking the average of each of the damping measurement at each strain amplitude.

Figure 33 demonstrates more clearly the difference between room temperature and 400 °F tests. The elevated temperature tests had a more rapid change in damping while the room temperature tests had a more gradual loss of damping. This combined with the difference in end state, shows that elevated temperature did have some effect on the loss of damping as well as the frequency change during the endurance testing.

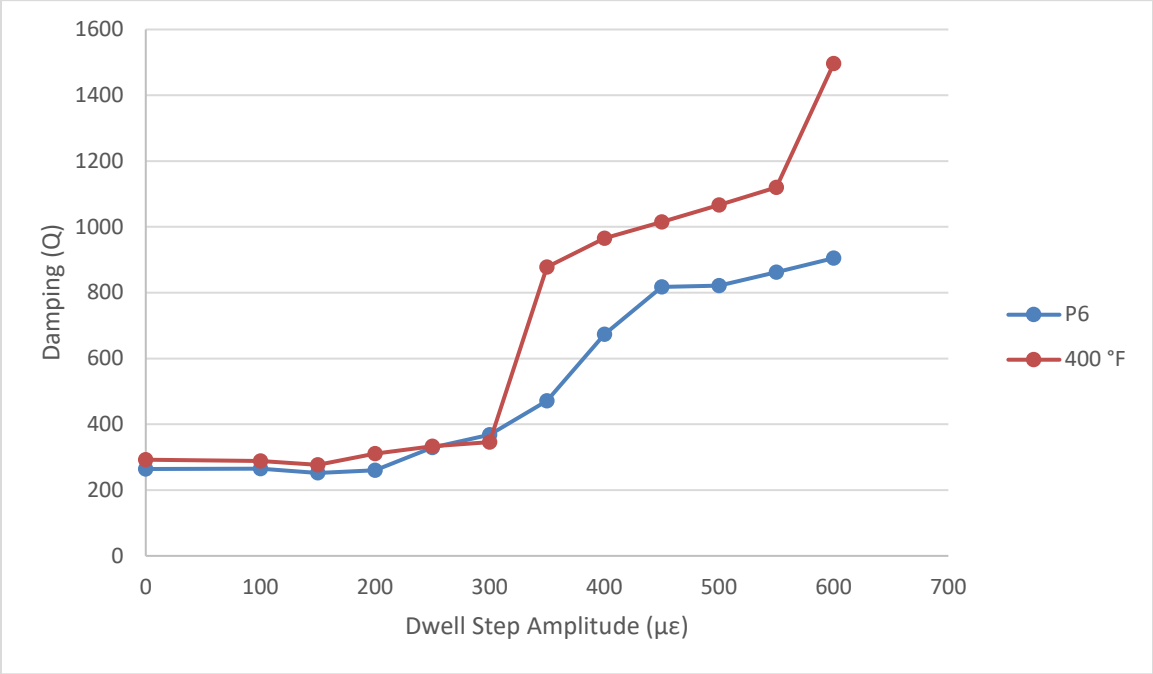

Figure 33: Average 400 °F Blade Compared with P6

Mode Shape Analysis

MAC tests were also performed in the same manner as described in Chapter 3. All post-test blade MACs are see in Figure 34. This shows that just like in room temperature, no real divergence from mode shape was seen.

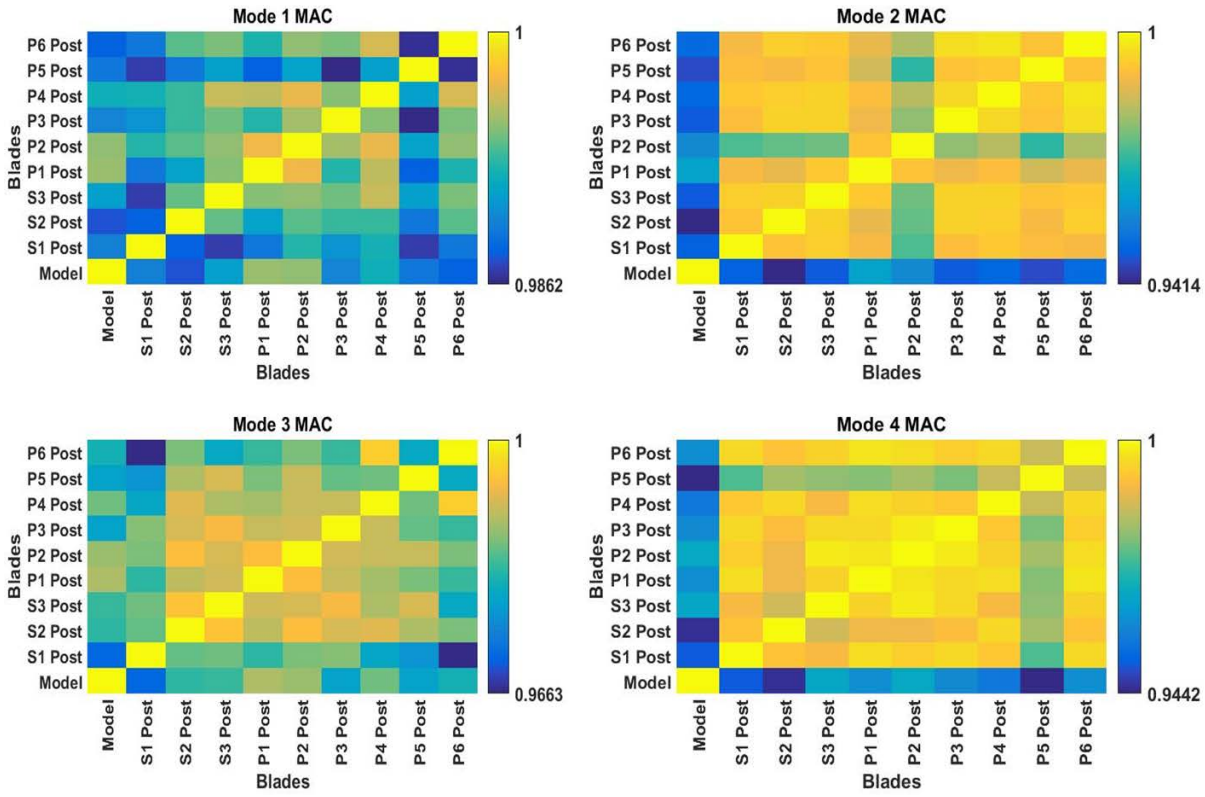

Figure 34: MAC All Blades Post Testing

This can also be shown with the Pre-test and Post-test together as seen in Figure 35. This shows that post-tests did deviate slightly from the pre-tests mostly in mode 1 and 3 (1st bend and 1st torsion respectively) when viewed as a family of blades. When the MAC is performed on each blade's data from pre- endurance to post- endurance testing a minimum MAC of 0.9815 (P6 mode 2) was found, show in Table 12. Despite the loss of damping quality, results demonstrate at least 98% similarity between pre and post damping endurance testing. This analysis demonstrates how the robustness of this technology and how the mode shape will not vary outside of expectations for what would be seen in a standard rotor setup.

Table 12: Direct Pre-Endurance to Post-Endurance Mac for All 6 Blades Modes 1-4

MAC	Mode 1	Mode 2	Mode 3	Mode 4
S1	0.9907	0.9908	0.9871	0.9981
S2	0.9932	0.9937	0.9944	0.9908
S3	0.9945	0.9921	0.9929	0.9971
P1	0.9996	0.9985	0.9979	0.9993
P2	0.9875	0.9901	0.9779	0.9942
P3	0.9928	0.9902	0.9899	0.9958
P4	0.9946	0.9910	0.9905	0.9927
P5	0.9896	0.9865	0.9858	0.9733
P6	0.9890	0.9815	0.9840	0.9905

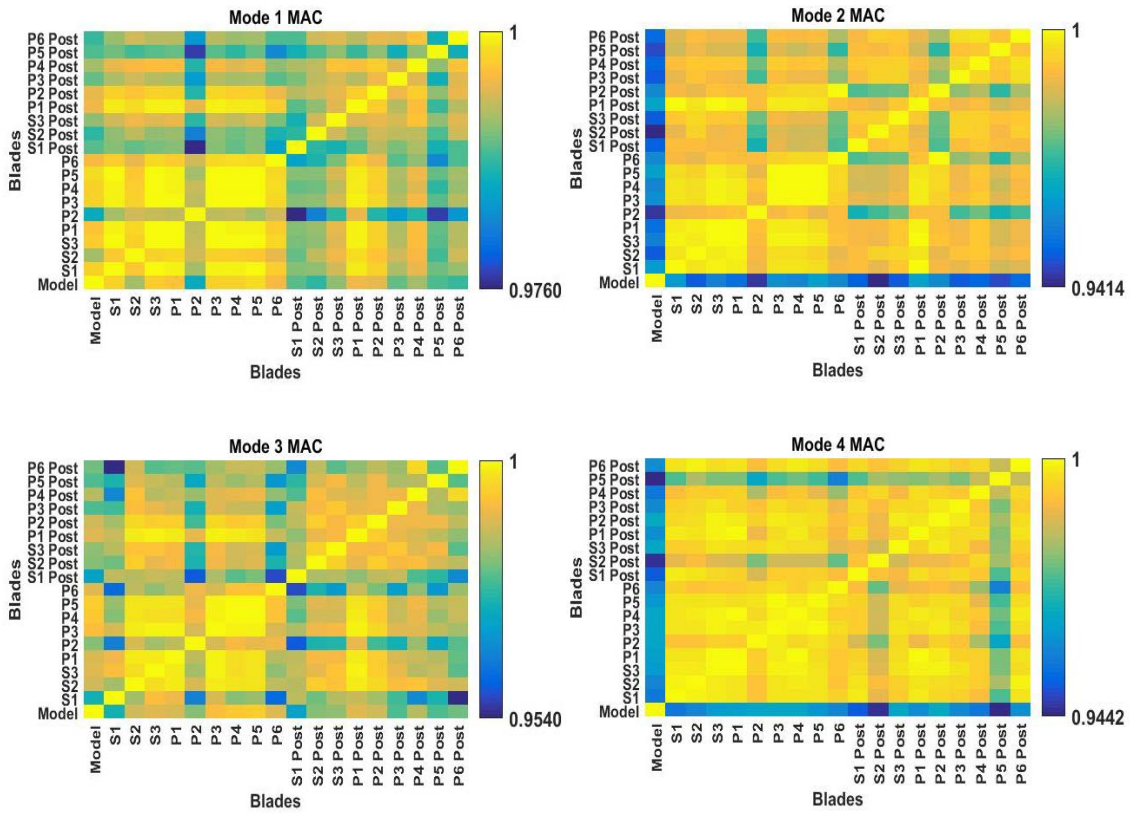

Figure 35: MAC All Blades Pre and Post Test

Post-Test Geometric Investigation

After all testing was performed the blades were again structured light scanned to investigate if any of the testing caused deformation of the blades. This was performed by scanning the blades using the structured light scanning and generating a 'heat plot' comparing the pre-test to the post-test scans. Blade P1, one of the blades that exhibited crack indications, showed some clear deformation. This is seen in Figure 36. These deviations are shown on the suction side root and the pressure side root and/or tip. The deviations shown on the suction side are small and likely caused by small changes in the location of the surface roughness peaks and valleys. The pressure side tip deflection is clear and spread through the trailing edge tip. These deviation shown are still very small

and the circular deviations across the part are actually the reference stickers used in the scanning process. All of the other blades showed no deviation when compared. While the deformation show in Figure 36 are measurable, it did not affect mode shape and the blade will be investigated further to identify if the crack is detectable without destruction.

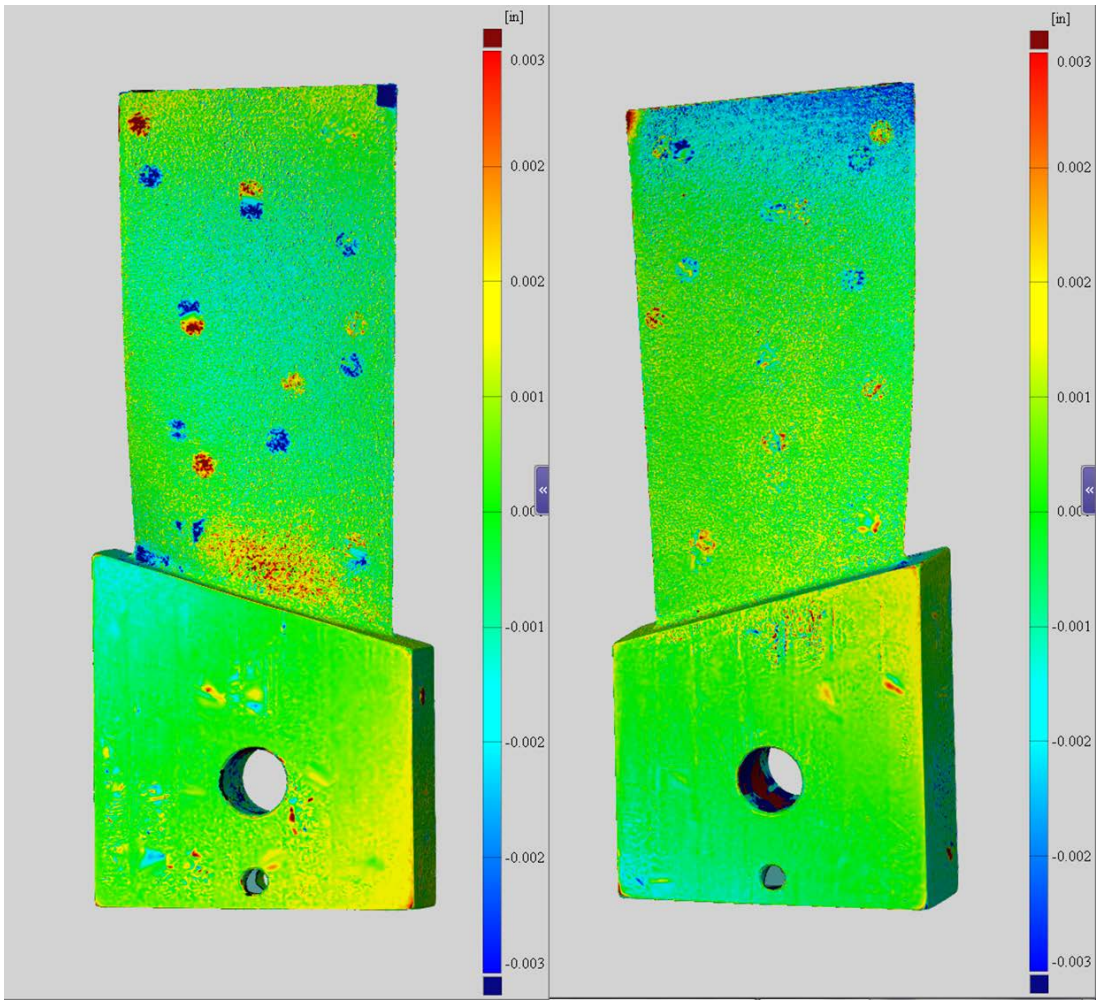

Figure 36: Structured Light of Blade P1 Pre-Test vs Post-Test. (Suction Side Left, Pressure Side Right)

Investigative Questions Answered

The results mentioned above have answered the fundamental research questions posed in Chapter 1. The blades with pockets showed significate damping (80-83%

vibration suppression) in their tests, this answers questions 1. The strain limitation was evaluated and found to be in the range of 350με - 500με. However, as noted in prior research even after these strain limitation the pocketed blades still have significantly better vibratory response suppression, requiring 1.45 times the input base excitation (or 31-42% vibration suppression) to achieve the same strain level at room temperature. At elevated temperature, the final damping relationship was reversed due to the high damping present in the solid blade taken at temperature. If the pocketed blades were compared to the other solid blades it is expected that phenomenon would be equivalent after the 600με step. However, the main objective or question of this paper was still achieved as, in practice and industry, the primary desire is to reduce total energy. To reach the point that the loss of damping quality was noted requires significantly more energy when this technology is applied.

Summary

This chapter outlined the results of the experimentation undertaken. The results show that the inclusion of the powder pocket technology into complex structure is possible and still, without optimization, operates with similar quality to that in beams. The next chapter will outline the research conclusions and thoughts on the technology and its many applications.

V. Conclusions and Recommendations

Chapter Overview

This research met all of the research objectives and in the process assisted the TEFF in creating a testbed gas turbine engine blade for this and other ongoing research. To apply this to turbine engines, an extreme environment both in temperature and force, more research is needed but other applications are now possible with the current level of knowledge. This chapter will summarize the author's thoughts on applications and where added effort is needed.

Conclusions of Research

The AM method described herein allows for the easy production of HCF resistant components. This method will allow for low cost and rapid manufacturing of these components by taking advantage of the quicker turnaround time of AM, specifically Laser Powder Bed Fusion (LPBF). This thesis outlines a few of the hurdles to understand. First the damping quality of this novel concept when applied to a complex structure (Turbine Engine Blade). Second how this behavior changes when done at elevated, turbine engine fan relevant, temperatures.

The turbine engine blades show similar damping quality to that seen in prior beam work. The 80-83% forced response reduction is slightly lower than that seen in beams but the pocket size and placement is not yet optimized. This demonstrates that this technology can be applied to complex structures.

The temperature testing showed similar initial damping as seen in room temperature. The main difference observed is a steep loss of damping at 350με which ended with solid blade equivalent damping by the end of the endurance testing.

All of this still shows the applicability of this technology. The results delineated in Chapter 4 shows that powder pockets can be easily added to components to give benefits of reduced vibratory response. In gas turbine engines more work is required, specifically in LCF life, to immediately apply but thanks to the manufacture speed of AM this can be done rapidly.

Significance of Research

This research has provided invaluable insight, and lays the framework into a new and emerging novel technology for rapid additive manufacturing. While this research focused specifically on gas turbine engine components it can be applied to innumerable other structural components. The study herein showed significant vibratory stress reduction that has opened up the door for applying the technology to everything from gas turbine engines to automotive parts to space based satellites. This groundbreaking technology could greenlight rapid prototype and fielding on a new level by mitigating issues related to vibratory stress. When applied to turbine engines LCF still need to be taken into account but many other applications do not require that type of testing and simply need strength testing for immediate application. The rapid manufacturing ability of AM can now be harnessed by a wide range of communities. The most beneficial part is that many AM applications are designed to have internal voids to lower weight and must find a way to get rid of the powder inside, this research shows instead they can

create a pocket for the powder and gain these vibratory strain reduction effects while still maintaining lower then fully fused density.

Research found in Chapter 2 shows the drive from the U.S. Air Force perspective to gain a damping mechanism in gas turbine parts. However all of these methods added weight and/or significant complexity in manufacturing. This powder pocket technology combats both of these weaknesses. In addition, since particle dampers were successfully tested by NASA in a centrifugally loaded test it alludes that these powder pockets will similarly still be successful in spinning applications. Altogether, it shows that this technology is of particular note to gas turbine engine applications.

Recommendations for Action

Advancements in this technology are still needed and some component specific research is required prior to application to specialized fields. However, the future research suggested below for continuing the path for application to rotating gas turbine engine hardware, arguably one of the most extreme and complicated environments this technology could be applied to.

"More Nations know how to build nuclear weapons than know how to make advanced turbine engines" -Dr. Greg Bloch DR-IV Chief Engineer AFRL/RQT

This quote is easily checked and true. This shows the complex nature of applying any technology to Turbine engines due to its environment. More research and tests are needed before this can be directly applied. Since AM has a shorter manufacturing process this can be done swiftly when funding and effort are applied.

Recommendations for Future Research

Overall this show that this technology is relevant and can be rapidly applied to complex structures. However, to truly apply this technology to maximum potency there are more areas that need understanding for gas turbine applications:

1. Optimization of pocket placement
2. Optimization of pocket shape
3. Centrifugal loading (spin-pit tests)
4. Build Parameter Optimization
5. LCF implications

(At this point engine tests could be performed and application to expendable equipment could be started. The added topics below would allow for better understanding of the technology)

6. Powder Interaction within the pocket (both Powder-Powder and Powder-wall)
7. FEA Model

Summary

With those areas not-withstanding, this study shows that it is possibly to simply apply this technology to a component and receive significant benefits. This method of passive damping does not result in added weight, increased HCF risk in other modes, complex architectural changes or one of the many other negatives discussed for other possible passive damping systems in Chapter 2. This demonstrates the utility of this technology and while more development is required this research allows another step

forward for its implementation, not only into engine components for test/rig or operational engines, but also other complex and simple aerospace structures.

Bibliography

American Soc. for Testing and Materials International. (2017). E756-05: Standard Test Method for Measuring Vibration-Damping Properties of Materials. In *ASTM Book of Standards.* West Conshohocken, PA: American Soc. for Testing and Materials International.

Bartsch, T. M. (2001). *High Cycle Fatigue (HCF) Science and Technology Program 2000 Annual Report.* Dayton, OH: Universal Technology Corporation.

Bartsch, T. M. (2002). *High Cycle Fatigue (HCF) Science and Technology Program 2001 Annual Report.* Dayton, OH: Universal Technology Corporation.

Bartsch, T. M. (2003). *High Cycle Fatigue (HCF) Science and Technology Program 2002 Annual Report.* Dayton, OH: Universal Technology Corporation.

Bruns, J. (2014). Fatigue Crack Growth Behavior of Structures Subject to Vibratory Stresses. *Society of Experimental Mechanics Annual Conference.* Greenville, SC.

D'Souza, K. X., & Epureanu, B. I. (2012). A Statistical Characterization of the Effects of Mistuning in Multistage Bladed Disks. *ASME, J. Eng. Gas Turbines Power*, pp 134.

Danforth, C. (1975). Blade Vibration: Some Key Elements in Design Verification. *Journal of Aircraft*, pp 333–342.

Els, D. (2011). Damping of Rotating Beams with Particle Dampers: Experimental Analysis. *AIAA Journal*, pp 2228–2238.

Ewins, D. J. (1984). Applications. In *Modal Testing: Theory and Practice* (pp. 217-251). New York: John Wiley & Sons Inc.

Fecke, T. G., Garretson, T., Zimmer, W., Webb, A., Roth, P., Larsen, A., . . . Coppedge, B. (2005). *Propulsion System High Cycle Fatigue Test Protocol Best Practice.* Dayton, OH: Propulsion Center of Excellence.

George, T., Seidt, J., Shen, M., Cross, C., & Nicholas, T. (2004). Development of a Novel Vibration-Based Fatigue Testing Methodology. *International Journal of Fatigue*, pp 477-486.

Gillaugh, D. L., Kaszynski, A. A., Brown, J. M., Beck, J. A., & Slater, J. C. (2019). Mistuning Evaluation Comparison Via As-Manufactured Models, Traveling

Wave Excitation, and Compressor Rigs. *ASME, J. Eng. Gas Turbines Power*, pp 141.

Jones, D., & Parin, M. (1972). Technique for Measuring Damping Properties of Thin Viscoelastic Layers. *Journal of Sound and Vibration*, pp 201-210.

Lopez, I., Busturia, J., & Nijmeijer, H. (2004). Energy Dissipation of a Friction Damper. *Journal of Sound and Vibration*, pp 539–561.

Micro Measurements. (2014). Strain Gage Rosettes: Selection, Applicaiton and Data Reduction. *Tech Note TN-515*, 5.

Naik, P., Lehmayr, B., Homeier, S., Klaus, M., & Vogt, D. M. (2019). Influence of Turbocharger Turbine Blade Geometry on Vibratory Blade Stresses. *ASME. J. Eng. Gas Turbines Power*, pp 141.

Nashif, A. D., Jones, D., & Henderson, J. P. (1985). *Vibration Damping.* New York: Wiley.

Nashif, A., Torvik, P., Desai, U., Hansel, J., & Henderson, J. (2008). Increasing Gas Turbine Blade Damping Through Cavities Filled with Viscoelastic Materials. *Journal of Propulsion and Power*, pp 741–750.

Nicholas, T. (2006). *High Cycle Fatigue: A Mechanics of Materials Perspective.* Oxford, UK: Elsevier.

Olson, S. (2003). An Analytical Particle Damping Model. *Journal or Sound and Vibration*, pp 1155–1166.

Panossian, H. (1991). Structural Damping Enhancement via Non-Obstructive Particle Damping Technique. *Journal of Vibration and Acoustics*, pp 101–105.

Reed, S. (2007). *Development of Experimental, Analytical, and Computational Techniques Appropriate for Nonlinear Damping Coatings.* Air Force Inst. of Technology: Ph.D. thesis, Dept. of Aeronautics and Astronautics.

Schnoes, M., & Nicke, E. (2017). A Database of Optimal Airfoils for Axial Compressor Throughflow Design. *ASME Journal Of Turbomachinery*.

Scott-Emuakpor, O., George, T., & Runyon, B. (2018 Pending).

Scott-Emuakpor, O., George, T., Runyon, B., & O'Hara, R. (2018). Strain Dependence of Inherent Damping in 3D Printed Inconel 718. *Vibration Institute Annual Training Conference.* Oak Brook, IL.

Scott-Emuakpor, o., George, T., Runyon, B., & Sheridan, L. (3-6 June 2019). Erosion and Life Inspection of Inherently Damped Components Subjected to Vibration Bending. *Society of Experimental Mechanics Annual Conference.* Reno, NV.

Scott-Emuakpor, O., George, T., Runyon, B., Beck, J., Sheridan, L., & Holycross, C. (2019). Sustainability Study of Inherent Damping in Additively Manufactured Nickel Alloy. *AIAA Journal*, pp 456-461.

Scott-Emuakpor, O., George, T., Runyon, B., Holycross, C., Langley, B., Sheridan, L., . . . Beck, J. (2018). Investigating Damping Performance of Laser Powder Bed Fused Components with Unique Internal Structures. *ASME/Turbo Expo, American Soc. Of Mechanical Engineers*, (pp. GT2018-75977). New York.

Scott-Emuakpor, O., George, T., Runyon, B., Langley, B., Sheridan, L., Holycross, C., . . . Johnson, P. (2018). Forced-Response Verification of Unique Additive Manufactured Vibration Suppressed Specimens. *Society of Experimental Mechanics Annual Conference, Soc. of Experimental Mechanics*, (p. Paper 794). Bethel, CT.

Scott-Emuakpor, O., Langley, B., Holycross, C., George, T., Runyon, B., & Justice, J. (2016). Comparison between Forced-Response and Hysteretic Energy Damping Assessment Methods. *AIAA Science and Technology Forum and Exposition* (pp. 2016-0666). AIAA Paper.

Scott-Emuakpor, O., Shen, M.-H., George, T., & Cross, C. (2008). A Energy-Based Uniaxial Fatigue Life Prediction Method for Commonly Used Gas Turbine Engine Materials. *ASME Journal of Engineering for Gas Turbines and Power*, Paper No. 062504.

Scott-Emuakpor, O., Sheridan, L., Runyon, B., & George, T. (2020). Vibration Fatigue Assessment of Additive Manufactured Nickel Alloy with Inherent Damping. *ASME/Turbo Expo*, (pp. GT2020-14122). London, England.

Sinha, A., & Griffin, J. (1983). Friction Damping of Flutter in Gas Turbine Engine Airfoils. *Journal of Aircraft*, pp 372–376.

Torvik, P. J. (2010). Damping Properties of Hard Coatings for Engine Applications. *Advances in Science and Technology*, pp 126–135.

Torvik, P. J. (2011). On Estimating System Damping from Frequency Response Bandwidths. *Journal of Sound and Vibration*, pp 6088–6097.

Torvik, P. J., Patsias, S., & Tomlinson, G. R. (2002). Characterizing the Damping Behaviour of Hard Coatings: A Comparison from Two Methodologies. *Proceedings of the 7th National Turbine Engine High Cycle Fatigue Conference.*

Torvik, P., & Langley, B. (2015). Material Properties of Hard Coatings Developed for High Damping. *AIAA Joint Propulsion Conference and Exposition* (pp. 2015-4195). AIAA Paper.

Torvik, P., Wilson, R., & and Hansel, J. (2007,). Influence of a Viscoelastic Surface Infiltrate on the Damping Properties of Plasma Spray Alumina Coatings, Part I: Room Temperature. *Proceedings of the Materials Science and Technology Conference and Exhibition*, (pp. 139–150).

U.S. Air Force. (2002, February). Engine Structural Integrity Program,. *MIL HDBK-1783B.*

REPORT DOCUMENTATION PAGE

Form Approved
OMB No. 074-0188

1. REPORT DATE *(DD-MM-YYYY)*	**2. REPORT TYPE**	**3. DATES COVERED** *(From – To)*
26-03-2020	Master's Thesis	September 2019 – March 2020

TITLE AND SUBTITLE

Structural Dynamic and Inherent Damping Characterization of Additively Manufactured Airfoil Components

5a. CONTRACT NUMBER

5b. GRANT NUMBER

5c. PROGRAM ELEMENT NUMBER

6. AUTHOR(S)

Goldin, Andrew, W., 1st Lt, USAF

5d. PROJECT NUMBER

5e. TASK NUMBER

5f. WORK UNIT NUMBER

7. PERFORMING ORGANIZATION NAMES(S) AND ADDRESS(S)
Air Force Institute of Technology
Graduate School of Engineering and Management (AFIT/ENY)
2950 Hobson Way, Building 640
WPAFB OH 45433-8865

8. PERFORMING ORGANIZATION REPORT NUMBER

AFIT-ENY-MS-20-M-263

9. SPONSORING/MONITORING AGENCY NAME(S) AND ADDRESS(ES)
Air Force Research Laboratory Turbine Integrity Branch
937-656-5530 and tommy.george@us.af.mil
ATTN: POC
Dr. Tommy George

10. SPONSOR/MONITOR'S ACRONYM(S)

11. SPONSOR/MONITOR'S REPORT NUMBER(S)

12. DISTRIBUTION/AVAILABILITY STATEMENT

13. SUPPLEMENTARY NOTES
This material is declared a work of the U.S. Government and is not subject to copyright protection in the United States.

14. ABSTRACT

The push for low cost and higher performance/efficient turbine engines have introduced a new demand for novel technologies to improve robustness to vibrations resulting in High Cycle Fatigue (HCF). There have been many proposed solutions to this, some passive and some active. With the advent of Additive Manufacturing (AM), new damping techniques can now be incorporated directly into the design and manufacture process to suppress the vibrations that create HCF. In this study, this novel unfused pocket damping technology is applied to a blade structure and the resulting damping effectiveness is quantified. The application of this technology to complex geometries will provide insight into both the underlying damping mechanism and its overall effectiveness. The finished blades are then computed tomography scanned to determine the as manufactured fill volume and to verify initial powdered locations. In this paper, first the damping quality is investigated when this technology is applied to a fan-like blade. Second, the strain limitations are investigated to understand limitations at room and elevated temperature. This research allowed an initial evaluation of the effectiveness of this technology to turbine engine fans as well as highlighting the overall effectiveness of this type of passive damping.

15. SUBJECT TERMS
Vibration, Damping, Modal Analysis, MAC, Additive Manufacturing, Laser Powder Bed Fusion

16. SECURITY CLASSIFICATION OF:			**17. LIMITATION OF ABSTRACT**	**18. NUMBER OF PAGES**	**19a. NAME OF RESPONSIBLE PERSON**
a. REPORT	**b. ABSTRACT**	**c. THIS PAGE**			Dr. Richard Cobb, AFIT/ENY
U	**U**	**U**	**UU**	88	**19b. TELEPHONE NUMBER** *(Include area code)* (937) 255-2184, (NOT DSN) (andrew.goldin@afit.edu)